Angewandte Reviews

E. Oldfield and W. Wang

DOI: 10.1002/anie.201306712

Bioorganometallic Chemistry

Bioorganometallic Chemistry with IspG and IspH: Structure, Function, and Inhibition of the [Fe_4S_4] Proteins Involved in Isoprenoid Biosynthesis

*Weixue Wang and Eric Oldfield**

Keywords:
bioinorganic chemistry · biophysics · enzyme catalysis · EPR spectroscopy · terpenoids

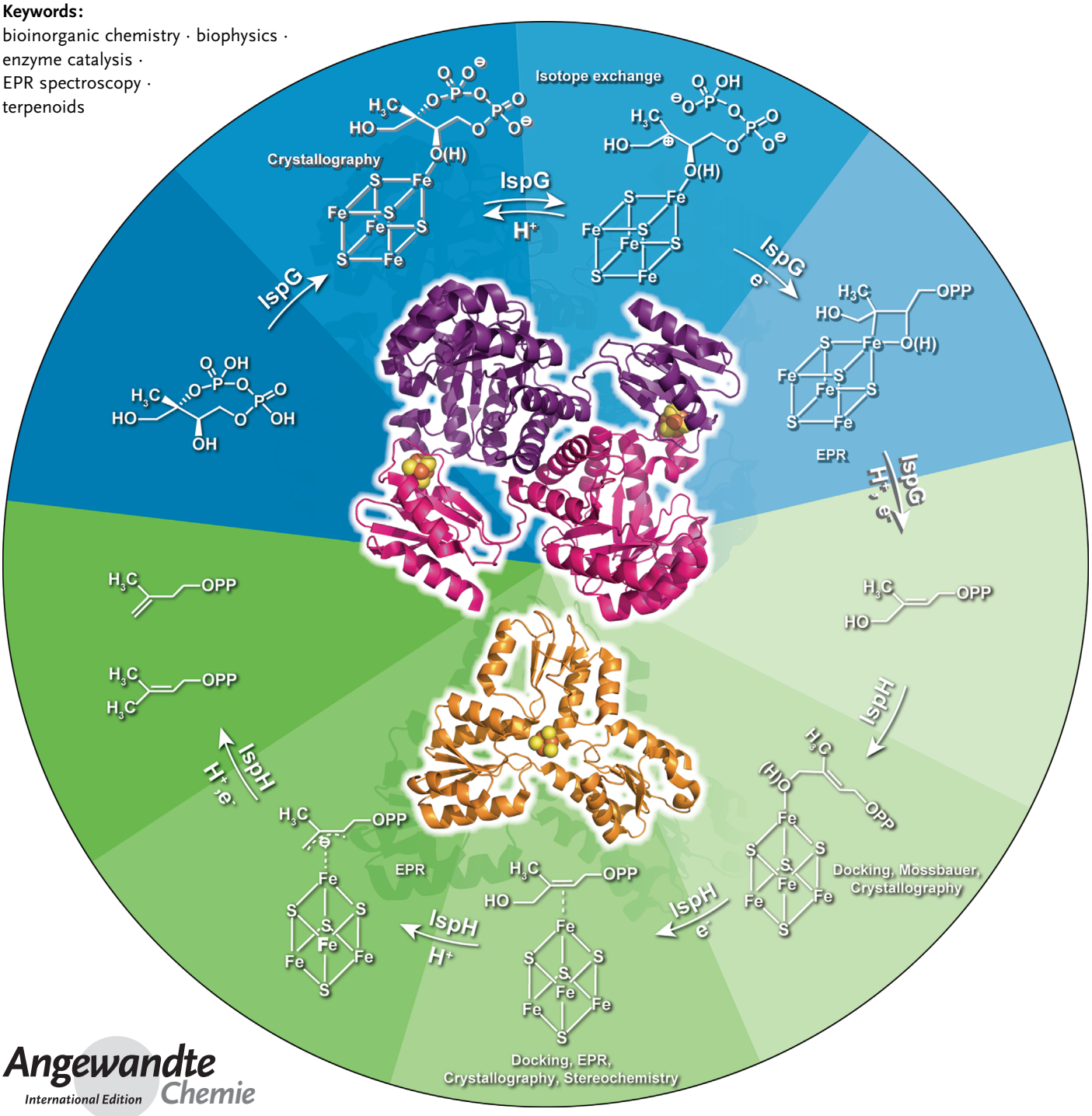

Enzymes of the methylerythritol phosphate pathway of isoprenoid biosynthesis are attractive anti-infective drug targets. The last two enzymes of this pathway, IspG and IspH, are [Fe_4S_4] proteins that are not produced by humans and catalyze 2 H^+/2 e^- reductions with novel mechanisms. In this Review, we summarize recent advances in structural, mechanistic, and inhibitory studies of these two enzymes. In particular, mechanistic proposals involving bioorganometallic intermediates are presented, and compared with other mechanistic possibilities. In addition, inhibitors based on substrate analogues as well as developed by rational design and compound-library screening, are discussed. The results presented support bioorganometallic catalytic mechanisms for IspG and IspH, and open up new routes to anti-infective drug design targeting [Fe_4S_4] clusters in proteins.

From the Contents

1. Introduction

Iron–sulfur proteins containing [Fe_4S_4] clusters[1] carry out a remarkably diverse series of reactions ranging from electron transfer (in ferredoxins)[2,3] to dehydration/isomerization (in, for example, aconitase in the Krebs cycle)[4,5] and free-radical reactions catalyzed by enzymes belonging to the radical-SAM (*S*-adenosylmethionine) superfamily.[6] More recently, another class of [Fe_4S_4] proteins was discovered that catalyze the formation of two key intermediates in isoprenoid biosynthesis: isopentenyl diphosphate (IPP, **1**; Scheme 1) and dimethylallyl diphosphate (DMAPP, **2**). The reactions

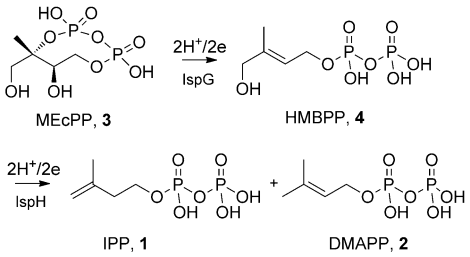

Scheme 1. Reactions catalyzed by IspG and IspH.

involved are the 2 H^+/2 e^- reduction of 2-*C*-methyl-D-erythritol-2,4-*cyclo*-diphosphate (MEcPP, **3**) to (*E*)-1-hydroxy-2-methylbut-2-enyl-4-diphosphate (HMBPP, **4**), catalyzed by IspG (also known as GcpE), and the 2 H^+/2 e^- reduction of **4** to form **1** and **2**, catalyzed by IspH (also known as LytB). IspG and IspH are both present in the methylerythritol phosphate (MEP) isoprenoid biosynthetic pathway (also known as the non-mevalonate pathway) discovered some 20 years ago,[7] and are essential for the survival of most bacteria as well as of malaria parasites, *Plasmodium* spp., because **1** and **2** are used in the formation of the undecaprenyl and decaprenyl diphosphates used in bacterial cell-wall biosynthesis, as well as in quinone biosynthesis and protein prenylation.[7–9] Since this pathway is absent in humans (who use the mevalonate pathway for isoprenoid biosynthesis), both IspG and IspH are of interest as new drug targets.[10] Both proteins are also present in the plastids of plants, where they are involved in quinone, chlorophyll (phytol), and carotenoid biosynthesis[8,11] and are, therefore, targets for new herbicides.[11] How these proteins function has, however, been a mystery for many years, since they need to catalyze both electron-transfer reactions (like ferredoxins) as well as substrate dehydroxylation.

In this Review, we cover three main topics: 1) the structures of IspG and IspH, 2) the catalytic mechanisms of IspG and IspH, and 3) the inhibition of IspG and IspH. The results described support a direct role of the [Fe_4S_4] cluster in catalysis as well as inhibition. Specifically, the unique fourth Fe center of the [Fe_4S_4] cluster is involved in the formation of "bioorganometallic" π, η^3-allyl, or ferraoxetane reaction intermediates, and inhibitors also bind to (and in some cases, react with) the [Fe_4S_4] clusters. These results lead not only to unique enzyme-catalyzed reaction mechanisms, but also give clues for the development of novel inhibitors as new drug (and herbicide) leads.

2. Structures of IspH and IspG

2.1. Historical Background, Activity, and Bioinformatics

In early studies, Adam et al. showed that IspH proteins contain three highly conserved cysteine residues (Figure 1 a)

[*] Prof. Dr. E. Oldfield
Department of Chemistry and Center for Biophysics and Computational Biology, University of Illinois at Urbana-Champaign
600 South Mathews Avenue, Urbana, IL 61801 (USA)
E-mail: eo@chad.scs.uiuc.edu
Dr. W. Wang
Department of Chemistry, Massachusetts Institute of Technology
77 Massachusetts Avenue, Cambridge, MA 02139 (USA)

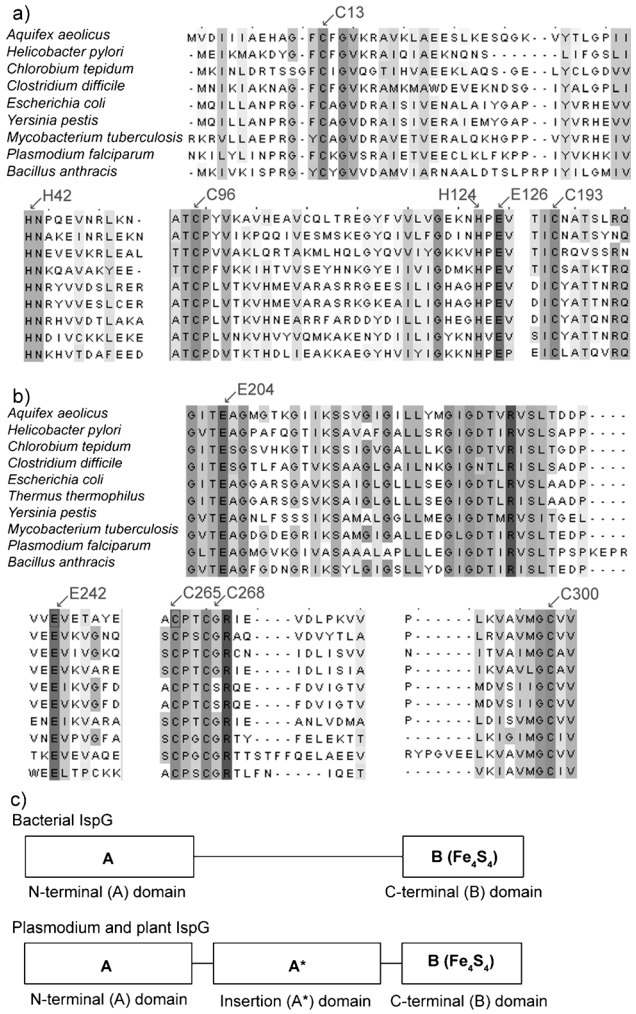

Figure 1. Bioinformatics analysis of IspH and IspG. a) Multiple-sequence alignment for IspH. b) Multiple-sequence alignment for IspG. c) Schematic view of the organization of the IspG domains.

that might be involved in iron–sulfur-cluster binding.[12] On the basis of the broad absorption around 420 nm of purified IspH from *Aquifex aeolicus*, the presence of an iron–sulfur cluster was also proposed by Altincicek et al.[13] Although the question of whether IspH harbors an $[Fe_4S_4]$[14,15] or an $[Fe_3S_4]$[16] cluster was controversial in early studies (discussed in more detail in Section 2.2), the realization that an iron–sulfur cluster was essential for catalysis rapidly led to the use of iron–sulfur-cluster reconstitution[14] or *isc*-operon coexpression[16] as well as anaerobic experimental conditions, which significantly increased IspH activity. Furthermore, several reduction systems were explored, including NAD(P)H/flavodoxin/flavodoxin reductase (or ferredoxin),[14–16] NADPH/ferredoxin/ferredoxin–$NADP^+$ reductase,[17] and methyl viologen/dithionite,[13,17] as well as photoreduction catalyzed by deazaflavin.[14–16] Later, even higher activities were achieved by the use of dithionite and artificial electron mediators.[18] Typical IspH activities are summarized in Table 1.

To identify other functionally important residues, we used the JPRED3 server[22] to produce an alignment of 461 IspH sequences from different organisms, then used this alignment as input to the SCORECONS server,[23] which produces an overall residue "conservation score" ranging from 1.000

Table 1: Recently reported activities of IspH.

Source	Reduction system and reaction condition	Specific activity [μmol mg^{-1} min^{-1}]	K_M [μM]	K_{cat} [s^{-1}]	Ref.
E. coli	dithionite, methyl viologen, pH 8.0, 37 °C	16.3	19.7	9.54	[18]
E. coli	dithionite, 6,7-dihydro-2,11-dimethyldipyrido[1,2-*a*:2,1-*c*]pyrazinium dibromide, pH 8.0, 37 °C	30.4	31.6	17.6	[18]
E. coli	dithionite, methyl viologen, pH 7.5	45 ± 3.6	n.d.	26.1 ± 2.1	[19]
E. coli	NADPH,[a] flavodoxin reductase, flavodoxin, pH 8.0, 37 °C	0.8	1	0.46	[20]
A. aeolicus	dithionite, methyl viologen, pH 8.0, room temperature	1.95	6.4	1.04	[21]

[a] NADPH is the reduced form of nicotinamide adenine dinucleotide phosphate.

Weixue Wang received his BSc in chemistry from Peking University, and a PhD in Biophysics and Computational Biology from the University of Illinois at Urbana-Champaign, where he was an American Heart Association Predoctoral Fellow under the direction of Eric Oldfield. He is now a postdoctoral associate with Stephen J. Lippard at the Massachusetts Institute of Technology. His research interests are in biosynthesis, bioinorganic chemistry and spectroscopy.

Eric Oldfield received a BSc in chemistry from Bristol University and a PhD in biophysical chemistry from Sheffield University under the direction of Dennis Chapman. He then worked as an EMBO Fellow at Indiana University with Adam Allerhand and at MIT with John Waugh. He joined the Chemistry Department at the University of Illinois at Urbana-Champaign in 1975 and is currently the Harriet A. Harlin Professor of Chemistry. His research interests are in drug discovery and spectroscopy.

Table 2: Some of the highly conserved residues in IspH (*E. coli* numbering). The activity data of IspH mutants are from Ref. [19].

Residue	Conservation score	*E. coli* mutant	Activity
H124	0.984	H124N	<1.0%
E126	0.965	E126Q	<1.0%
S225	0.94	S225C	<1.0%
N227	0.938	N227Q	<4.4%

(most highly conserved) to 0 (not conserved). The JPRED3/SCORECONS results for some of the most highly conserved residues in *A. aeolicus* IspH are shown in Table 2. Besides the three Cys residues required for $[Fe_4S_4]$-cluster binding, H124, E126, S221, and N223 (H124, E126, S225, and N227 in *Escherichia coli* IspH) were found to have very high conservation scores, and these residues are indeed essential for IspH catalysis according to the results of site-directed mutagenesis.[19,24]

In the case of IspG, in a very early study, mechanisms similar to those of vitamin K epoxyquinone reductase or ribonucleotide reductase were proposed.[25] It was then found that IspG was an iron–sulfur enzyme with three conserved Cys residues coordinated to a $[Fe_4S_4]$ cluster.[14,26] As for IspH, several redox systems have been used for IspG-activity assays, including NAD(P)H/flavodoxin/flavodoxin reductase,[26–28] methyl viologen/dithionite,[29–32] and photoreduction by deazaflavin[15,26,27] or by a thylakoid preparation from spinach chloroplasts for the plant (*A. thaliana*) IspG.[28] Some recently reported IspG activities are listed in Table 3.

Table 3: Recently reported activities of IspG.

Source	Reduction system and reaction condition	Specific Activity [μmol mg^{-1} min^{-1}]	K_M [μM]	K_{cat} [s^{-1}]	Ref.
E. coli	dithionite, methyl viologen, pH 8.0, 37°C	0.55	311 ± 21	0.395	[29]
A. aeolicus	dithionite, methyl viologen, pH 9.0	2.5 (60°C); 11.3 (90°C)	n.d.	1.6 (60°C); 7.4 (90°C)	[30]
T. thermophilus	dithionite, methyl viologen, pH 8.0, room temperature	0.124	8	0.09	[31]

There are two different classes of IspG enzymes. In most bacteria, multiple-sequence alignment revealed that there are three conserved cysteine residues (Figure 1b) and two major domains (A, B; Figure 1c) containing numerous conserved residues. SCORECONS analysis[23] indicated that E204 (*A. aeolicus* numbering; 232 in *Thermus thermophilus*) is one of the most conserved residues, consistent with mutagenesis results.[30,33]

In plants (e.g. *Arabidopsis thaliana*), malaria parasites (e.g. *Plasmodium falciparum*), and several other bacteria (such as *Chlorobium tepidum* and *Chlamydia trachomatis*), bioinformatics analysis revealed not two but three domains: A, A*, and B (Figure 1c).[33,34] The A* domains have about the same overall length as the A domains, but there are essentially no conserved amino acids in the different A* sequences. This observation suggests a primarily structural as opposed to a more direct, catalytic role, for the A* domain. The questions then arise: What are the three-dimensional structures of IspH and of the two-domain and three-domain IspGs? Where are the essential residues? How are they involved in catalysis?

2.2. X-ray Crystallographic Investigations of the IspH Structure

The first X-ray crystallographic structure of an IspH was reported by Rekittke et al. for the *Aquifex aeolicus* protein (PDB: 3DNF),[35] and was followed shortly after by the structure reported by Gräwert et al. for the *E. coli* protein (PDB: 3F7T).[19] In both cases, it was found that the protein adopted a "trefoil" fold with three α/β domains surrounding a central $[Fe_3S_4]$ cluster (Figure 2a). On the basis of previous

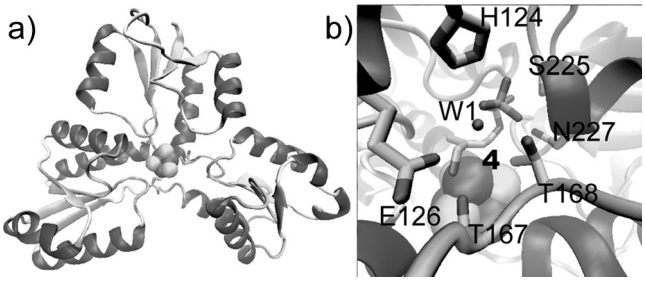

Figure 2. X-ray crystal structures of IspH. a) Ligand-free *A. aeolicus* IspH, which shows a trefoil fold with a $[Fe_3S_4]$ cluster at the center (PDB: 3DNF).[35] b) *E. coli* IspH with bound **4**; the structure shows that **4** forms an alkoxide complex with the $[Fe_4S_4]$ cluster (PDB: 3KE8).[36] Some of the key residues at the active site are shown. Figures were prepared with the software package VMD.[38]

studies in which electron paramagnetic resonance (EPR) spectroscopy was used,[14] it was suggested that the crystallographically observed $[Fe_3S_4]$ cluster was actually an artifact caused by the loss of one Fe atom from a $[Fe_4S_4]$ cluster during crystallization. The $[Fe_4S_4(Cys)_3]$ coordination motif is the same as that found in aconitase[4] and suggests that substrate **4** might coordinate to the unique fourth Fe atom to facilitate the electron-transfer/reductive-dehydroxylation steps. In a docking study, the fourth Fe atom was computationally "reconstituted", and it was proposed that the substrate **4** bound to the 4th Fe center through O1 to form an alkoxide complex.[35] Indeed, the X-ray crystallographic structure of IspH containing an $[Fe_4S_4]$ cluster with bound **4** (PDB: 3KE8) later obtained by Gräwert et al.[36] supports this proposal, as do the results of Mössbauer spectroscopy.[37] This ligand-bound structure showed a more closed conformation than that found in the absence of the ligand, with the totally

conserved E126 residue located in close proximity to the [Fe_4S_4] cluster as well as to the hydroxy group of **4**. The diphosphate moiety was hydrogen bonded to a series of polar residues, including highly conserved H124, S225, and N227 (H124, S221, and N223 in *A. aeolicus* IspH), as shown in Figure 2b.

2.3. X-ray Crystallographic and Electron Microscopic Investigations of the IspG Structure

Two years after the first reports on IspH structures, Lee et al. obtained the crystal structure of IspG from *A. aeolicus* (PDB: 3NOY),[30] a two-domain (AB) IspG, and a report by Rekittke et al.[39] of the structure of IspG from *T. thermophilus* (PDB: 2Y0F), another two-domain protein, soon followed. *A. aeolicus* IspG actually crystallizes as a dimer, $(AB)_2$ (Figure 3a). The A (N-terminal) domain belongs to the TIM-barrel superfamily[40] and has closest structural identity to dihydropteroate synthase,[41] whereas the B (C-terminal) domain houses the [Fe_4S_4] cluster and consists of a fold that is similar to those seen in sulfite reductase[42] and the ferredoxin domains of nitrite reductase.[43] One glutamate (E350 in *T. thermophilus*; E307 in *A. aeolicus*) and three cysteine residues of the B domain coordinate to the [Fe_4S_4] cluster. The distances between the putative active sites in an AB monomer are very large (ca. 40 Å), and both research groups proposed that only the dimers would be active, since they could adopt a head-to-tail structure (Figure 3a,b) in which the active sites would be formed from the A domain of one monomer and the B domain of the second monomer; a "hinge-bend" or opening/closing motion during catalysis would enable substrate/product ingress/egress. This proposal was recently confirmed by Rekittke et al. by the solution of a **3**-bound IspG structure (PDB: 4G9P; Figure 3b,c) in which the diphosphate group of **3** clearly binds to the A domain of one molecule in the dimer, whereas the C3 OH group coordinates to the unique fourth Fe atom in the [Fe_4S_4] cluster in the B domain of the second molecule in the dimer (Figure 3c) and thus initiates catalysis.[44]

To date, no X-ray crystallographic structure of a three-domain IspG has been reported. However, Liu et al. reported that the results of structure prediction with six different programs all indicated that the A* or "insert" domain in several three-domain IspGs would also be expected to adopt a TIM-barrel fold,[33] just as found in the A domains. The results suggested a three-domain A(TIM)–A*(TIM)–B-(Fe_4S_4) structure (Figure 1c) in which all conserved residues are in the A and B domains. This structural proposal received support from the results of single-particle electron tomography (Figure 3d), which showed that the homology model (for *A. thaliana* IspG) fits well into the electron density observed by electron microscopy.[33] Thus, the catalytic mechanisms for the two-domain and three-domain IspGs are expected to be the same, with the only difference that the three-domain protein has an extra A* domain, which plays a primarily structural role.

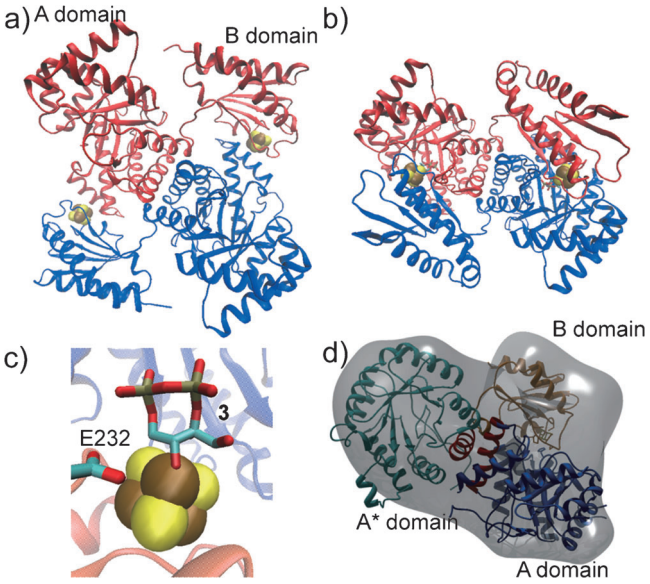

Figure 3. Structures of IspGs. a) Ligand-free *T. thermophilus* IspG (PDB: 2Y0F).[39] b) *T. thermophilus* IspG with bound **3** (PDB: 4G9P).[44] c) MEcPP (**3**) binds to the [Fe_4S_4] cluster through O3 to form an alkoxide complex; the highly conserved residue E232 is 3.7 Å away from O3.[44] d) A model of the three-domain IspG from *A. thaliana* docked into a 20 Å electron-density map created by single-particle electron tomography of *A. thaliana* IspG.[33] Images (a–c) were prepared by using VMD.[38] Image (d) was adapted from Ref. [33] with permission.

2.4. Investigation of Active-Site Iron–Sulfur Clusters by Mössbauer Spectroscopy

The electronic structure and ligand coordination of the iron–sulfur cluster at the active sites of IspG and IspH have been directly probed by ^{57}Fe Mössbauer spectroscopy. Seemann et al. first reported a Mössbauer spectroscopic study of ^{57}Fe-reconstituted oxidized ([Fe_4S_4]$^{2+}$) IspGs from *A. thaliana* (a three-domain plant protein; Figure 4a) and *E. coli* (a two-domain protein; Figure 4b).[45] Their results clearly showed that the two- and three-domain proteins had extremely similar Mössbauer spectra characteristic of [Fe_4S_4] clusters. In particular, there was a 3:1 signal-intensity ratio, proposed to arise from three tetrahedral-sulfur-coordinated $Fe^{2.5+}$ sites and one $Fe^{2.5}$ site with one non-cysteine (N or O) ligand as well as three sulfur ligands. This proposal is consistent with later X-ray crystallographic observations[44] that the fourth ligand in oxidized IspG is a glutamate.

In the case of IspH, the Mössbauer spectroscopic results for the oxidized protein were rather different to those reported for IspG, in that there were now three iron sites with a 2:1:1 intensity ratio (Figure 4c).[18,37] Site 1 was characteristic of tetrahedrally sulfur coordinated $Fe^{2.5+}$ centers of mixed-valence iron pairs with a delocalized excess electron. Site 2 was characteristic of a high-spin ferric iron, whereas site 3 was characteristic of a high-spin ferrous iron. Upon comparison with other [Fe_4S_4] proteins with known coordination geometries, it was proposed that oxidized IspH contains 3 S and 3 N/O ligands,[37] although the actual nature of the N/O-containing ligands still remains to be determined.

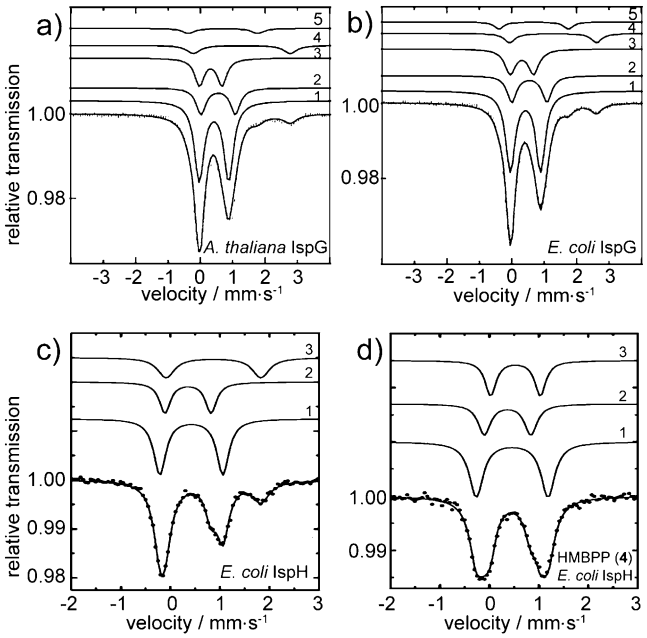

Figure 4. Mössbauer spectra of IspG and IspH. a) Mössbauer spectrum of ^{57}Fe-reconstituted *A. thaliana* IspG (356 μM) obtained at $T = 77$ K.[45] b) Mössbauer spectrum of ^{57}Fe-reconstituted *E. coli* IspG (413 μM) obtained at $T = 77$ K.[45] Spectra were adapted from Ref. [45] with permission from Springer Science and Business Media. c) Mössbauer spectrum of *E. coli* IspH obtained at $T = 77$ K.[37] d) Mössbauer spectrum of *E. coli* IspH with **4** bound obtained at $T = 77$ K.[37] Spectra were adapted from Ref. [37] with permission. Copyright (2009) American Chemical Society.

More importantly, on the binding of substrate **4** to the oxidized protein, the isomer shift of the third component (high-spin Fe^{2+}) decreased, from $\delta_3 = 0.89\ mm\,s^{-1}$ to $\delta_3 = 0.53\ mm\,s^{-1}$, thus showing that **4** binds to the unique fourth Fe atom, since the other spectral components did not change (Figure 4d), in agreement with the earlier computational predictions.[35] The same results were obtained with *E. coli* cells overproducing IspH and thus provided strong support for the idea that the active site of IspH (in cells) contains an $[Fe_4S_4]$ cluster, not an $[Fe_3S_4]$ cluster.[37]

These bioinformatic, X-ray crystallographic, and Mössbauer spectroscopic investigations led to detailed, but essentially "static" pictures of the IspH and IspG structure. To understand how these two enzymes catalyze $2\,H^+/2\,e^-$ reductions, transient species (i.e. reaction intermediates) need to be trapped and characterized. By taking advantage of the paramagnetic nature of reduced $[Fe_4S_4]$ clusters, electron paramagnetic resonance (EPR) spectroscopy has played an important role in revealing the identities of several reaction intermediates trapped during catalysis, and combined with the results from X-ray crystallographic, stereochemical, and other experimental (and theoretical) studies has led to detailed mechanistic proposals for IspH as well as IspG catalysis, and in turn to the inhibition of these enzymes.

3. The Catalytic Mechanism of IspH

How IspH catalyzes the "reductive dehydroxylation" of HMBPP (**4**) has been a mystery for nearly a decade, and seven mechanisms have been proposed, with carbocation, carbanion, and carbon-radical reaction intermediates.[13–15,19,46–49] Recent spectroscopic studies found no evidence for any radical species[50] and point to a "bioorganometallic" mechanism involving direct iron–carbon interactions during catalysis,[24,50] as summarized in Scheme 2. The trapping and characterization of three putative intermediates led to reaction-mechanism proposals based on EPR spectroscopic studies and density functional theory (DFT) calculations as well as Mössbauer spectroscopic, X-ray crystallographic, and stereochemical results.

3.1. IspH Intermediate I: The Alkoxide Intermediate

To initiate the catalytic cycle, the substrate **4** first binds to the oxidized cluster ($[Fe_4S_4]^{2+}$) of IspH to form intermediate I

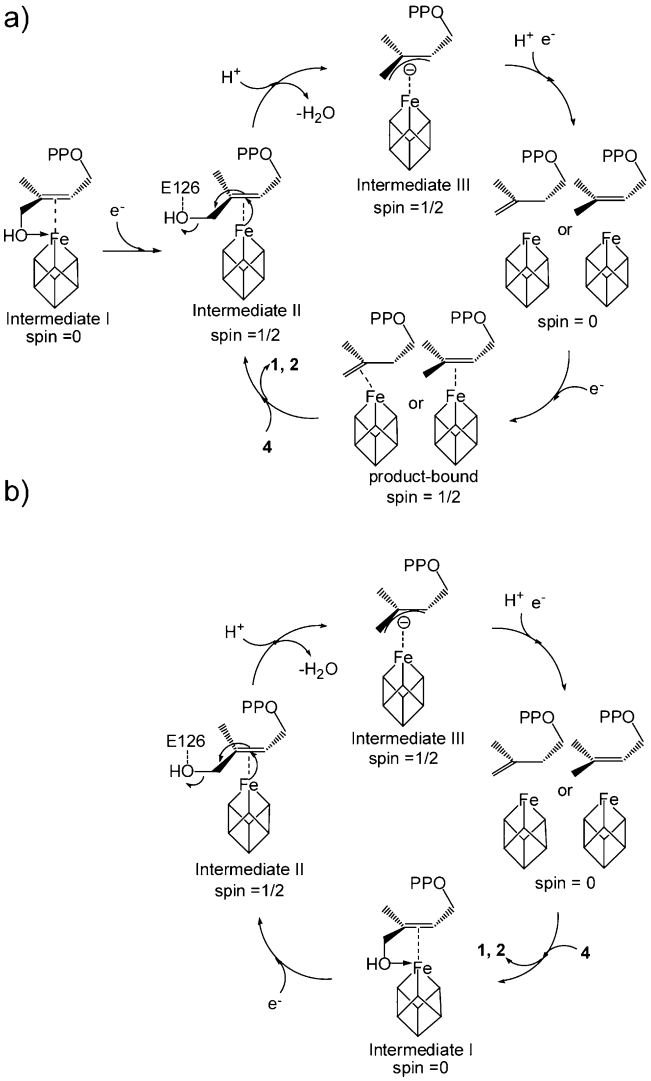

Scheme 2. The bioorganometallic mechanism of IspH catalysis. OPP represents the diphosphate group.

(Scheme 2). As discussed earlier, computational docking,[35] Mössbauer spectroscopy,[37,51] and X-ray crystallography[36] all indicate that this intermediate is an η^1-alkoxide (or alcoholate) complex. This species may (Scheme 2a), or may not (Scheme 2b), be involved in steady-state catalysis; in the latter scenario, IspH can be reduced by excess reductant right after the formation of product **1** or **2**. Substrate **4** then displaces the product and directly binds to the reduced $[Fe_4S_4]^+$ cluster, thus forming intermediate II and skipping intermediate I. Support for this possibility comes from the observation of the product-bound $[Fe_4S_4]^+$ cluster in an EPR study of steady-state catalysis when substrate **4** was consumed in the presence of excess reductant (see Ref. [24]). More experiments are required to determine which scenario is more likely.

3.2. IspH Intermediate II: The Weak π-Complex with a Rotated Hydroxymethyl Group

According to the originally proposed bioorganometallic mechanism for IspH catalysis,[24] when IspH is reduced, the hydroxymethyl group of **4** in intermediate I rotates away from the $[Fe_4S_4]^+$ cluster to interact with E126, a totally conserved residue proposed to serve as a proton donor,[35] to form intermediate II. This proposal is supported by the results of three experiments. First, rotation of the hydroxymethyl group has in fact now been observed in a crystal structure of a wild-type *E. coli* IspH:**4** complex that was first irradiated with X-rays.[52] In this experiment, the IspH:**4** complex was probably photoreduced by X-ray preirradiation; the hydroxymethyl group of **4** then dissociated from the unique fourth iron center and rotated away from the cluster to form a hydrogen bond with the diphosphate group of **4** as well as E126 (Figure 5a). Second, an intermediate was trapped by using an IspH E126Q or E126A mutant (Figure 5b).[24,50] The hyperfine sublevel correlation (HYSCORE) spectrum, a two-dimensional pulsed EPR spectrum, of this intermediate prepared with [1-^{17}O]**4** showed a ^{17}O hyperfine interaction of only about 1 MHz (Figure 5c).[50] This interaction is much smaller than the ^{17}O hyperfine interactions found in systems containing direct Fe–O bonds, such as aconitase, which are characterized by ^{17}O hyperfine coupling constants in the 8–15 MHz range.[53,54] The small ^{17}O hyperfine coupling indicates that the terminal hydroxy group of **4** does not bind to the reduced cluster ($[Fe_4S_4]^+$), in agreement with the crystal structure of the IspH:**4** complex after X-ray preirradiation. The third experiment that supports this critical rotation was reported by Dickschat and co-workers,[55] who used ^{2}H-isotopic labeling and found that the observed *E*/*Z*-^{2}H labeling pattern in product **1** necessitated removal of the hydroxymethyl group from the cluster with the rotation. The rotation is critical from a mechanistic perspective, since this step is absent in the radical[48] and ferraoxetane[21] models (see below) for IspH catalysis. Further studies are required to establish the kinetic competency of this intermediate in the reaction catalyzed by wild-type IspH, but clearly computational docking, EPR spectroscopy, and the results of X-ray crystallography all suggest that this critical rotation occurs, and E126 is a better proton source than T167, which was proposed as the proton source in the Birch reduction type mechanism.[48,49]

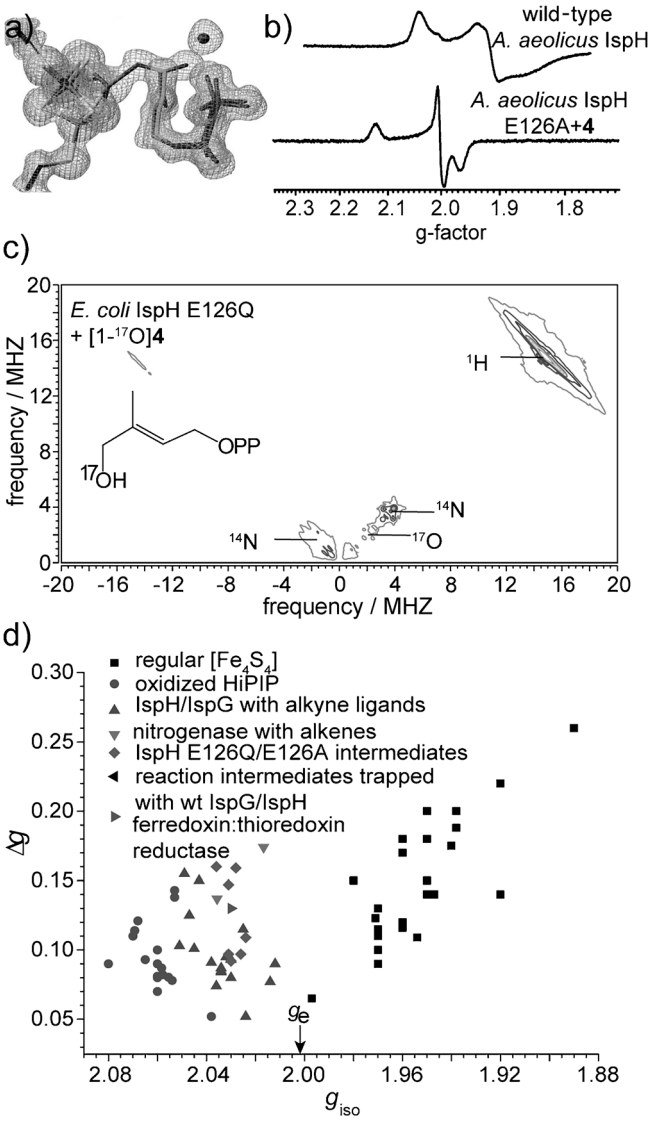

Figure 5. Intermediate II of IspH catalysis. a) Intermediate II with a rotated hydroxymethyl group was observed together with the alkoxide complex with crystals preirradiated with X-rays. Reprinted from Ref. [52] with permission. Copyright (2011) Elsevier. b) EPR spectra of ligand-free *A. aeolicus* IspH (top) and intermediate II trapped with an E126A mutant. Adapted from Ref. [24] with permission. c) HYSCORE spectrum of intermediate II trapped with [1-^{17}O]**4**. d) Plot of g_{iso} versus Δg for 80 iron–sulfur containing systems. Spectrum and graph in (c) and (d) are adapted from Ref. [50] with permission. Copyright (2012) American Chemical Society. wt = wild-type.

An early EPR spectroscopic study[24] suggested that intermediate II is a π-complex, not a free radical. The similarity of the *g*-tensor of trapped intermediate II (Figure 5b; $g = [2.124, 1.999, 1.958]$)[24] to the values observed with an allyl alcohol bound nitrogenase α-70^{Ala} mutant ($g = [2.123, 1.998, 1.986]$)[56] suggested the possibility that the alkene substrate **4** formed a similar "σ/π-complex" to that reported for allyl alcohol bound to the nitrogenase α-70^{Ala} mutant.[56,57] In fact, comparison with the *g*-tensors of 80 other

$[Fe_4S_4]$-cluster-containing proteins and model complexes (Figure 5d) shows that the *g*-tensor of intermediate II is similar to those of systems that have alkene or alkyne ligands and is characterized by $g_{iso} > g_e$ (the free-electron *g*-value).[50] It is unlikely that intermediate II arises from a free radical in view of its highly anisotropic *g*-tensor as well as the results of an electron–nuclear double-resonance (ENDOR) study, which showed ^{57}Fe hyperfine coupling constants of 26 and 39 MHz for the two pairs of Fe atoms in the $[Fe_4S_4]$ cluster, but very small (ca. 1 MHz) ^{13}C hyperfine coupling constants for [U-$^{13}C_5$]**4**,[24] thus demonstrating that most of the spin density is located on the $[Fe_4S_4]$ cluster.

Taken together, the results described above indicate that intermediate II is a π-complex with the hydroxymethyl group rotated away from the reduced cluster ($[Fe_4S_4]^+$). Considering that the Fe–C distances (2.8–3.3 Å)[52] observed in the crystal structure are longer than those observed in classical organometallic π-complexes/metallacycles, together with the fact that the C2 and C3 carbon atoms are not pyramidalized as in, for example, Zeise's salt,[58] intermediate II is perhaps best described as a weak π- or van der Waals complex, and essentially "sets up" **4** in the active site for the next steps in the reaction.

3.3. IspH Intermediate III: The η^3-Allyl Complex

The terminal hydroxy group of **4** in intermediate II interacts with the proton donor E126. In the next catalytic step, this hydroxy group is protonated and removed as a water molecule with the formation of intermediate III. This intermediate has been trapped by the addition of **4** to one-electron-reduced IspH,[21,59] as well as by rapid freeze quenching of the reaction of wild-type IspH with **4** under steady-state conditions (Figure 6a),[50] and is characterized by an anisotropic *g*-tensor (e.g. $g = [2.173, 2.013, 1.997]$ for the intermediate trapped with *A. aeolicus* or *P. falciparum* IspH).[21] More detailed pre-steady-state kinetic studies are desirable to confirm the kinetic competence of this intermediate,[60] but the kinetics observed under steady-state conditions are consistent with the kinetics of the enzyme in the presence of methyl viologen. This intermediate disappeared within 5 s when dithionite (120 equiv), methyl viologen (1 equiv), and **4** (50 equiv) were used,[50] in agreement with the specific activity of 16.3 μmol mg^{-1} min^{-1}[18] and the k_{cat} value of 9.8 s^{-1} (Table 1). When methyl viologen is excluded from the reaction and dithionite is the sole reductant, the reaction is three orders of magnitude slower, and this intermediate can be observed for a much longer period of time, depending on the amount of substrate and reductant added.

The terminal hydroxy group is not present in this intermediate, as evidenced by the absence of any ^{17}O hyperfine interaction in the HYSCORE spectrum of samples prepared by using [1-^{17}O]**4**.[50,59] The spin-density distribution as revealed by the EPR spectroscopic data makes it unlikely that intermediate III is an allyl free radical. Moreover, the continuous-wave EPR spectrum was significantly broadened when ^{57}Fe-enriched IspH was used (Figure 6a), thus indicating that most spin density is located on the $[Fe_4S_4]$ cluster. This result is consistent with the small ^{13}C and ^{2}H hyperfine coupling constants observed for intermediate III (Figure 6b):[21,50,59] the ^{2}H and ^{13}C hyperfine coupling constants are more than 7 times (^{2}H) and 15 times (^{13}C) smaller than those expected for an allyl radical.[61]

The nature of intermediate III is further revealed by its *g*-tensor, which is characterized by $g_{iso} > g_e$. Such a *g*-tensor is unusual for a $[Fe_4S_4]^+$ cluster and is reminiscent of that of an oxidized high-potential iron–sulfur protein (HiPIP, $[Fe_4S_4]^{3+}$).[62] To understand the mechanistic implications of this unusual *g*-tensor, it is of interest to examine the catalytic mechanism of ferredoxin–thioredoxin reductase (FTR), a well-studied $[Fe_4S_4]$ enzyme that catalyzes the $2H^+/2e^-$ reduction of a disulfide bond.[63–65] As in the case of IspH, FTR generates an intermediate with $g_{iso} > g_e$ ($g = [2.11, 2.00, 1.98]$)[64] through a two-electron reduction of the disulfide bond by the reduced iron–sulfur cluster $[Fe_4S_4]^+$ to form a HiPIP-type $[Fe_4S_4]^{3+}$ cluster, thus avoiding the generation of a thiol free radical.[64,65] By analogy with this reaction, the HiPIP-like *g*-tensor of intermediate III suggests a two-electron reduction of **4** by the reduced iron–sulfur cluster ($[Fe_4S_4]^+$) during IspH catalysis and the resulting formation of an allyl anion complexed in an η^3 manner to the HiPIP-like $[Fe_4S_4]^{3+}$ cluster. However, it is also possible that proton transfer to the allyl anion occurs to form a product (**1** or **2**) complexed to the HiPIP cluster as intermediate III.

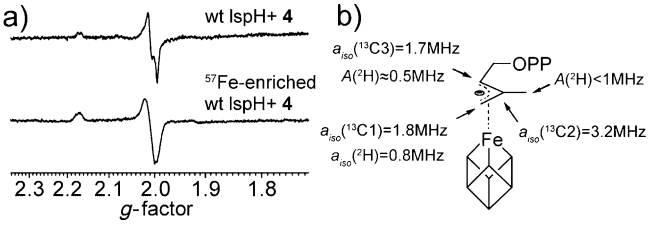

Figure 6. Intermediate III of IspH catalysis. a) X-band EPR spectrum of intermediate III trapped with natural-abundance or ^{57}Fe-enriched wild-type *E. coli* IspH. Adapted from Ref. [50] with permission. Copyright (2012) American Chemical Society. b) Hyperfine coupling constants of ligand atoms in intermediate III. The $a_{iso}(^2H)$ value for the deuterium atom on C1 was determined in Refs. [21, 50, 59].

3.4. Other Mechanistic Possibilities for IspH

Other proposed mechanisms can be categorized into two types: 1) mechanisms involving free-radical intermediates, as represented by the Birch reduction type mechanism (Scheme 3),[48,49] and 2) mechanisms involving other bioorganometallic species (Scheme 4).[21]

There are two difficulties associated with the Birch reduction type mechanism. First, the rotation of the hydroxymethyl group of **4** suggested by computational docking,[35] EPR spectroscopy,[50] and X-ray crystallography[52] and confirmed by an isotope-labeling stereochemical study[55] is absent in this mechanism. Instead, it is proposed that the terminal hydroxy group of **4** is protonated and removed by T167, a much weaker proton donor than E126. Second, the

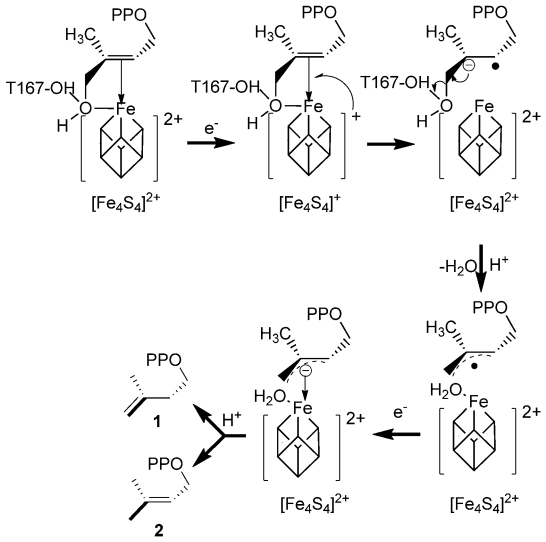

Scheme 3. The proposed Birch reduction type mechanism of IspH catalysis.[48,49] OPP represents the diphosphate group. Adapted from Ref. [50] with permission. Copyright (2012) American Chemical Society.

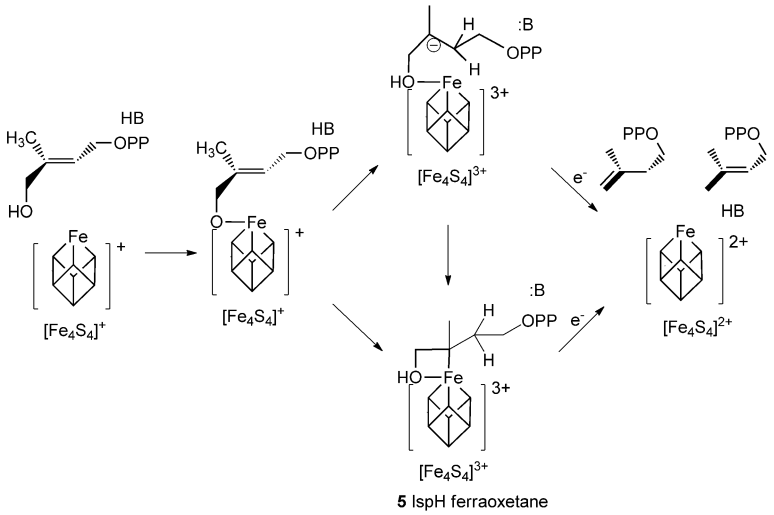

Scheme 4. The ferraoxetane mechanism for IspH catalysis.[21] Adapted from Refs. [21, 50] with permission. Copyright (2012) American Chemical Society.

proposed radical species have not been observed in any experiments, and the species that have been observed are not free radicals. Indeed, in quantum-chemical calculations,[59] we found that an $[Fe_4S_4]^{2+}$/radical cluster is less stable than a $[Fe_4S_4]^{3+}$/allyl anion; that is, an internal electron transfer occurs during geometry optimization.

To explain the nature of the $g_1 = 2.17$ reaction intermediate (intermediate III in our mechanism), another model featuring a ferraoxetane, **5** (Scheme 4), has been proposed.[21] This structure is very reminiscent of that proposed by us earlier for intermediate X in IspG catalysis (see below);[31,33,66,67] however, the involvement of the ferraoxetane **5** in the IspH reaction is inconsistent with several experimental observations, the most important being the absence of any ^{17}O hyperfine interaction in samples prepared with [1-^{17}O]**4**,[50] which rules out the possibility of an Fe–O bond. Furthermore, there is no evidence for any direct bonding interaction between the apical Fe atom and C2: the ^{13}C hyperfine coupling constants for C1, C2, and C3 are all small (1.8–3.2 MHz; Figure 6b) and can be reproduced by DFT calculations on a model η^3-allyl complex,[59] whereas the Fe–C2 ^{13}C hyperfine coupling in the IspG ferraoxetane is approximately 17 MHz.[67] Other difficulties with this model include the absence of the critical rotation of the hydroxymethyl group and its inability to explain the formation of product **2** or the reaction with a fluorinated substrate analogue, which does not form any Fe–F bond.[50,68]

4. The Catalytic Mechanism of IspG

In early studies, several mechanisms involving carbocations, carbanions, an epoxide, and carbon-radical reaction intermediates were proposed (Scheme 5).[15,26,32,69] The first three mechanisms shown in Scheme 5 share a carbocation as the first reaction intermediate. The importance of such an intermediate was later supported by isotope-exchange experiments with the [2-^{13}C,^{18}O]-labeled MEcPP substrate **6** (Scheme 6).[70] On the basis of the different chemical shifts of C2 when bonded to either ^{16}O or ^{18}O, it was demonstrated that on the addition of IspG and in the absence of any reductant, **6** can be converted into **7**, thus suggesting opening of the cyclodiphosphate ring and transient formation of the carbocationic species **8** (Scheme 6). The observed rate of conversion was, however, 63 times lower than the k_{cat} value of IspG for the catalysis of the reductive dehydroxylation of **3**, possibly as a result of the restricted rotation of the diphosphate group in **8**.[70]

An alternative mechanism, in which the formation of an epoxide intermediate initiates catalysis (Scheme 5d), was proposed by Rohdich et al.[15] This proposal was based on previous observations that an epoxide could be reduced to an ethylene group by a synthetic $[Fe_4S_4]$ cluster[71] and is supported by the fact that the epoxide **9** is indeed an IspG substrate (Scheme 7) with a k_{cat} value (20.1 min^{-1}) comparable to that of the natural substrate **3** (23.7 min^{-1}; Table 3).[72] Furthermore, **9** and **3** form the same paramagnetic intermediate (intermediate X; see below) when they react with IspG, as identified by EPR and ^1H ENDOR spectroscopy.[66] These results, do not, however, establish the intermediacy of **9** in the reductive dehydroxylation of **3** by IspG. Efforts to identify the formation of **9** from **3** under either oxidizing or reducing conditions were not successful, whereas the reverse reaction, the conversion of **9** into **3** under the catalysis of oxidized IspG ($k_{cat} \approx 2.0\ min^{-1}$) was observed.[73] Thus, it is likely that **9** is not normally involved in catalysis. Rather, both **9** and **3** can form the same reaction intermediate, intermediate X, which is then converted into **4**.

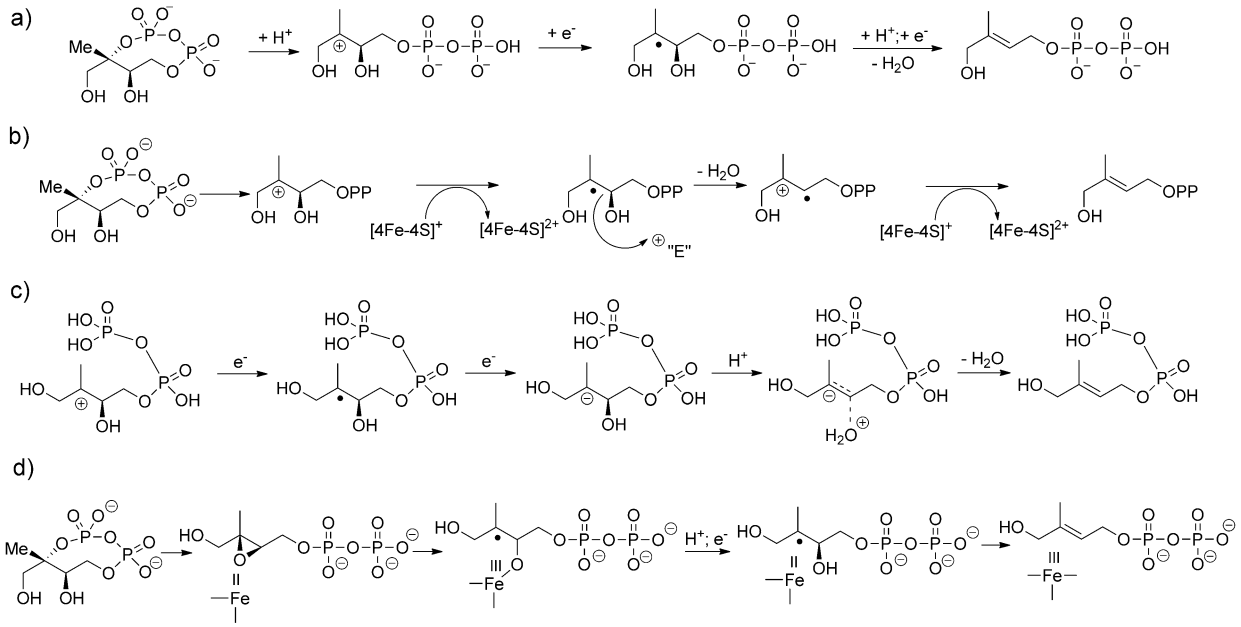

Scheme 5. Proposed reaction mechanisms of IspG catalysis. a) Cation → radical mechanism of Kollas et al.[32] b) Cation → radical → cation-radical mechanism of Seemann et al.[26] c) Cation → radical → anion mechanism of Brandt et al.[69] d) Oxirane → radical mechanism of Rohdich et al.[15]

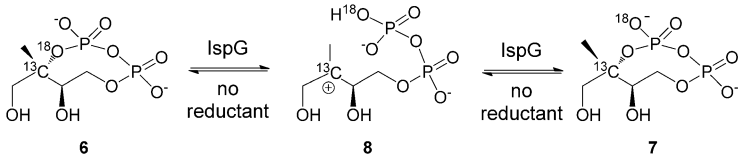

Scheme 6. Isotopic exchange of **6** (isotopically labeled **3**) as catalyzed by oxidized IspG.

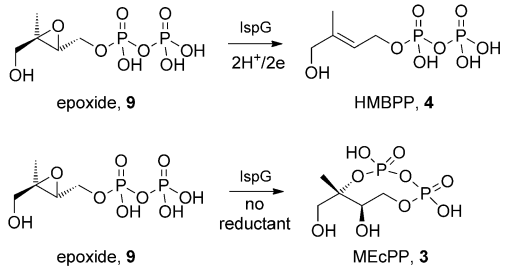

Scheme 7. Reactions of epoxide **9** with IspG.

The next reaction intermediate in the previously proposed mechanisms (Scheme 5) is a carbon free radical, but as with IspH, so far no radical species have been reported. A paramagnetic species characterized by $g = [2.087, 2.019, 2.000]$ (intermediate X; Figure 7a) was, however, observed by EPR spectroscopy in the freeze-quenched reaction of IspG with **3**[74] or with **9**.[66] However, it is unlikely to be a free radical, because its EPR spectrum broadened significantly upon trapping with ^{57}Fe-enriched IspG (Figure 7a), thus indicating that a large amount of spin density is located on the $[Fe_4S_4]$ cluster. More compelling evidence for the nature of intermediate X comes from extensive hyperfine-coupling-tensor measurements, which suggest that "X" is a ferraoxetane, an organometallic species containing both Fe–C and Fe–O bonds, as described in the following. Why a ferraoxetane? Such a species would appear to be highly strained, but high strain is not necessarily a problem for a reaction intermediate. Moreover, opening of the cyclodiphosphate ring would provide a possible site (C2) for binding to the unique fourth iron center of the $[Fe_4S_4]^+$ cluster to form an Fe–C bond.

Evidence for an Fe–C bond comes from ^{13}C-hyperfine-coupling measurements on intermediate X. A large ^{13}C hyperfine coupling was observed in the HYSCORE spectrum of X trapped with [U-$^{13}C_6$]-labeled **3**, with a hyperfine-coupling tensor $A(^{13}C) = [14.5, 12.0, 26.5]$ MHz (Figure 7b).[67] The 17.7 MHz isotropic hyperfine coupling constant $a_{iso}(^{13}C)$ is significantly larger than the $a_{iso}(^{13}C)$ values of 3.7 and 1.1 MHz observed for the nitrogenase:allyl alcohol complex, in which the allyl alcohol was proposed to bind directly to the FeMo cofactor to form a metallacycle with one of the Fe atoms.[56] It is comparable to the $a_{iso}(^{13}C)$ value of 17.1 MHz observed for ^{13}CO in CO-inhibited [FeFe] hydrogenase, in which CO directly binds to the H_{ox} cluster.[75] The strongly coupled carbon atom in X was specifically assigned as C2 (the quaternary carbon atom) by the use of [2,3-$^{13}C_2$]- and [1,3,4-$^{13}C_3$]-labeled **3**; its neighboring carbon atom (C3) has a much weaker hyperfine coupling constant ($a_{iso}(^{13}C) = 3.0$ MHz), and for all other carbon atoms, $a_{iso}(^{13}C) < 1$ MHz.[66,67]

Evidence for an Fe–O bond comes from ^{17}O HYSCORE studies of X prepared by the use of specifically ^{17}O-labeled substrates. Because the chemical synthesis of ^{17}O-labeled **9** is

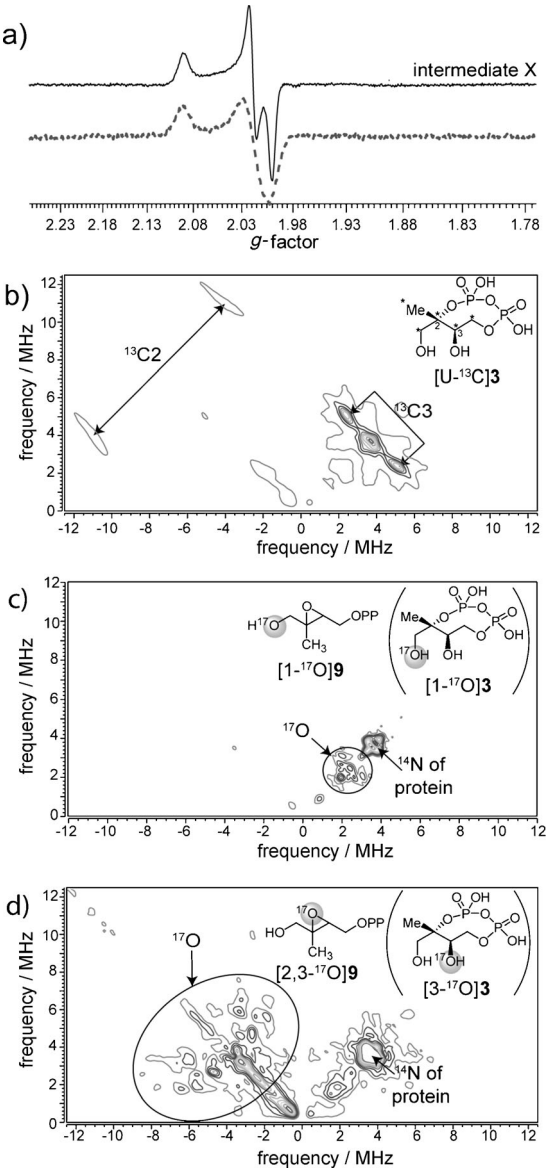

Figure 7. EPR spectroscopic characterization of intermediate X of *E. coli* IspG. a) Continuous-wave EPR spectrum of intermediate X. The dashed line is the intermediate trapped with ^{57}Fe-enriched IspG. b–d) HYSCORE spectra of intermediate X prepared with [U-^{13}C]**3** (b), [1-^{17}O]**9** (c), and [2,3-^{17}O]**9** (d). Adapted from Refs. [33, 66, 67] with permission.

much easier than that of ^{17}O-labeled **3**, and because **9** forms the same intermediate X as does **3**, [1-^{17}O]- and [2,3-^{17}O]-labeled **9** were synthesized and used to prepare "X". With [1-^{17}O]-labeled **9**, only a very small ^{17}O hyperfine coupling (ca. 0.15 MHz, by simulation; Figure 7c) was observed in intermediate X, whereas intermediate X prepared from [2,3-^{17}O]**9** exhibited a large ^{17}O hyperfine coupling (ca. 8 MHz; Figure 7d). The hyperfine coupling constant of about 8 MHz is comparable to that observed when $H_x{}^{17}O$ ($A(^{17}O) = 8$–12 MHz)[53] or ^{17}O-labeled substrates or substrate analogues ($A(^{17}O) = 9$–15 MHz)[54] are bonded to the unique iron atom (Fe_a) of aconitase. The ^{17}O-HYSCORE results thus indicate that the 3-OH group, but not the 1-OH group, of **3** directly binds to the unique fourth iron center of the [Fe_4S_4] cluster in X. This conclusion is strongly supported by the crystal structure of IspG complexed with **3**[44] (Figure 3c), in which there is an Fe–O3 bond (in the oxidized state of the iron–sulfur cluster).

The results of ^{13}C- and ^{17}O-hyperfine-coupling measurements indicate bonding of C2 and O3 to the [Fe_4S_4] cluster in intermediate X, thus narrowing down the possible structures for this species. The most likely candidate appears to be the ferraoxetane **10** (Scheme 8). Structure **10** may look unusual, but several metallaoxatanes are known as stable species.[76,77] Moreover, in the case of an interaction between iron and oxirane, the 1,2-ferraoxetane was observed by matrix isolation,[78] and on warming, the ferraoxetane underwent a [2+2] dissociation to ethylene and FeO.[78]

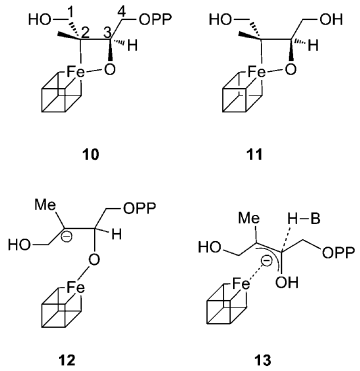

Scheme 8. Proposed structures **10**, **12**, and **13** for intermediate X and a model ferraoxetane **11** used for DFT calculations. OPP represents the diphosphate group.

The results of ^{31}P and ^{1}H ENDOR spectroscopy are also consistent with the assignment of X as the ferraoxetane **10**. The ^{31}P hyperfine-coupling tensor has been determined to be either a predominantly isotropic tensor ($A = [0.21,\ 0.09,\ 0.05]$ MHz) or a predominantly dipolar tensor ($A = [0.22,\ -0.11,\ -0.09]$ MHz).[31] In either case, the very small hyperfine couplings indicate that the diphosphate group does not bind to the iron–sulfur cluster. By the use of a point-dipole model, a minimum distance of 6.6 Å from the phosphorus nucleus to the unique fourth iron center was estimated on the basis of the predominantly dipolar tensor.[31] The ^{1}H hyperfine coupling constants of all hydrogen atoms derived from **3** were determined by ENDOR spectroscopy and selective ^{2}H-isotopic labeling.[67] The largest ^{1}H hyperfine coupling ($A(^{1}H) = [14, 11, 11]$ MHz)[31] in intermediate X was assigned to one of the hydrogen atoms of the C2′ methyl group; all other hydrogen atoms, including the other two hydrogen atoms of the C2′ methyl group, have much smaller hyperfine couplings.[67] The small anisotropy of the hyperfine tensor $A(^{1}H) = [14, 11, 11]$ MHz is consistent with the location of this hydrogen atom in the second coordination sphere of the [Fe_4S_4] cluster, where it experiences a weak dipolar interaction with the paramagnetic center. The large difference in the hyperfine coupling constants for the three hydrogen atoms in the C2′ methyl group was well reproduced by DFT

calculations on a model ferraoxetane **11** (see below),[33] further supporting this structural assignment.

A DFT calculation on the model ferraoxetane $[Fe_4S_4(SMe)_3\{-C(CH_2OH)(CH_3)CH(CH_2OH)O-\}]^{2-}$ (**11**; Scheme 8)[33] gave a reasonable set of predictions for the experimentally measured hyperfine coupling constants. In particular, the large difference in the hyperfine coupling constants for the three hydrogen atoms of the C2′ methyl group was reproduced, and was found to arise from the dependence of the hyperfine coupling constant on the H-C-C-Fe dihedral angle. The calculated large coupling ($A_i(^1H) = 9.1$ MHz) was in reasonable accord with the experimental result (12 MHz) and arose from the *trans* hydrogen atom (Fe-C-C-H torsion angle: 172°), whereas the smaller hyperfine couplings originated from the *gauche* (+/−) hydrogen atoms, with geometry-optimized torsion angles of 52 and −67°.[33] A similar dihedral-angle dependence of hyperfine coupling constants was observed for the C^β hydrogen atoms of cysteine ligands bound to $[Fe_4S_4]^+$ clusters;[79] this phenomenon is similar to the well-known observation of large ^3J *trans* scalar couplings in NMR spectroscopy.

There are two other structures that have been proposed for intermediate X:[31] the carbanions **12** and **13** (Scheme 8). Structure **12** is unlikely because a carbanion would not be expected to be stable (since CH groups have pK_a values of about 40), and more importantly, this structure would be inconsistent with the large hyperfine coupling constant observed for C2. Structure **13** is likewise unlikely: it is not an oxaallyl species (which might be stable) as a result of the protonation of the O atom, and ^{2}H-3 is not exchanged during isoprenoid biosynthesis.[80]

On the basis of these considerations and the results of isotope exchange,[70] X-ray crystallography,[30,39,44] and site-directed mutagenesis,[30,33] we propose the IspG mechanism shown in Scheme 9. The first step is the coordination of O3 (the oxygen atom to be removed as a water molecule) to the unique fourth iron atom of the oxidized iron–sulfur cluster ($[Fe_4S_4]^{2+}$) to form the alkoxide/alcoholate complex observed in the crystal structure of IspG cocrystallized with **3**.[44] This reaction is probably catalyzed by E232—the most highly conserved non-cysteine residue in IspG as based on SCONS analysis[23] and its close proximity to O3 in the IspG:**3** crystal structure.[44] The opening of the cyclodiphosphate ring and formation of the carbocation is reversible once **3** binds to the oxidized iron–sulfur cluster, as evidenced by the exchange of ^{18}O of [2-^{13}C,^{18}O]**3** in the presence of oxidized IspG.[70] When an electron is accepted from a reductant, a ferraoxetane (intermediate X) forms. Considering the HiPIP-like *g*-tensor with $g_{iso} = 2.035$, it seems likely that the one-electron-reduced iron–sulfur cluster ($[Fe_4S_4]^+$) performs a two-electron reduction of **3** to form the ferraoxetane, similar to that proposed for FTR and now IspH catalysis. The ferraoxetane then dissociates to the final product **4** and oxidized IspG by accepting one more electron and one more proton.

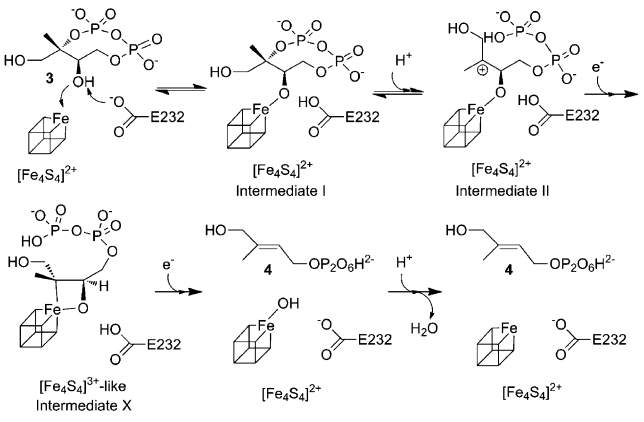

Scheme 9. Proposed mechanism of IspG catalysis based on the results of EPR spectroscopy, DFT calculations, and X-ray crystallography, as well as mutagenesis and isotope-exchange experiments.

5. Inhibitors of IspH and IspG

An important aspect of research on isoprenoid biosynthesis, including the MEP pathway, is the development of anti-infective drug leads.[10,81–83] The past three years have seen significant advancement in IspH- and IspG-inhibitor development, which has partially benefitted from the study of the catalytic mechanism: the first potent IspH and IspG inhibitors, alkyne diphosphates, were rationally designed on the basis of the proposed bioorganometallic catalytic mechanism of IspH. Up to now, three strategies have been employed for the development of IspH and IspG inhibitors: 1) the synthesis of substrate analogues, 2) mechanism-based rational design, and 3) compound-library screening. These strategies are summarized in Sections 5.1–5.3.

5.1. Substrate Analogues as Inhibitors

Substrate analogues that bind to IspG or IspH but cannot be turned over could be potent inhibitors of interest as new anti-infective drug leads and herbicides. Replacement of the diphosphate group with carbamate (compounds **14**), *N*-acyl-*N*′-oxysulfamate (compounds **15**), or aminosulfonyl carbamate groups (compounds **16**; Scheme 10) resulted in only weak inhibitory effects against IspH or IspG.[84] The substitution of the diphosphate group also abolished the ability of these compounds to activate human Vγ2Vδ2 T cells (**4** is an activator at ca. 30 pM).[85,86]

In contrast, substitution of the terminal hydroxy group with a thiol (compound **17**) or an amino group (compound **18**; Scheme 10) led to potent IspH inhibitors with IC_{50} values of

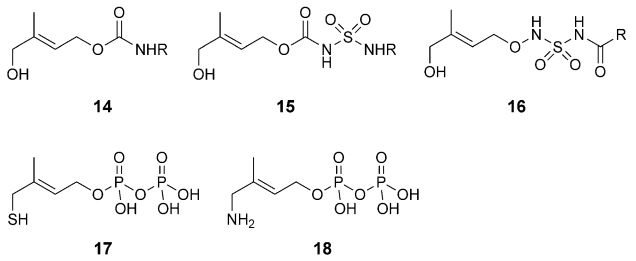

Scheme 10. Substrate analogues as IspH inhibitors.

0.21 and 0.15 μM, respectively, against IspH.[20,51] Both inhibitors were not turned over by IspH (unlike the fluoro analogues)[49,50] and underwent reversible binding with the terminal thiol or amino group coordinated to the unique fourth iron center to form complexes similar to the alkoxide complex observed with the natural substrate, **4**. Compound **18** was found to be a slow binding inhibitor, possibly owing to the deprotonation step required for binding to the $[Fe_4S_4]$ cluster.[20] Such binding modes were established by Mössbauer spectroscopy (Figure 8a,b) and DFT calculations,[51] and were later confirmed by X-ray crystallography (Figure 8c, PDB: 4H4E and Figure 8d, PDB: 4H4D).[68] With **18**, an additional conformation in which the aminomethyl group is rotated away from the $[Fe_4S_4]$ cluster was observed, perhaps as a result of photoreduction of the iron–sulfur cluster in the X-ray beam.[68] At present, it is not clear whether the inhibition of enzyme catalysis is due to the binding of inhibitors to the oxidized clusters, reduced clusters, or both.

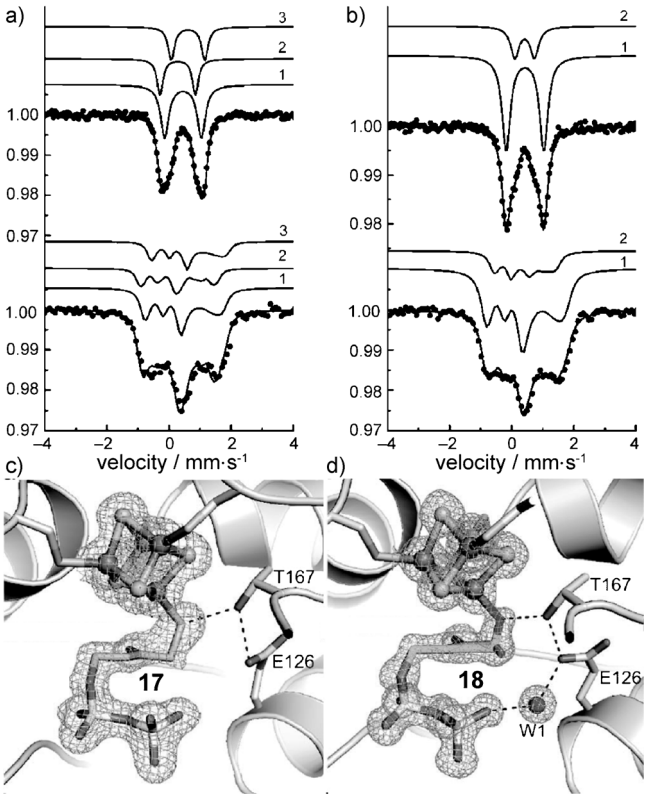

Figure 8. Binding of inhibitors **17** and **18** to *E. coli* IspH. a,b) Mössbauer spectra and simulated Mössbauer spectra of the binding of **17** (a) and **18** (b) to IspH ($T = 77$ K, $B = 0$ T for the top traces; $T = 5$ K, $B = 5$ T applied perpendicular to the γ beam for the bottom traces). Adapted from Ref. [51] with permission. Copyright (2013) American Chemical Society. c,d) Crystal structures of **17** and **18** complexed to IspH. Adapted from Ref. [68].

5.2. Rational Inhibitor Design Based on the IspH Catalytic Mechanism

The bioorganometallic mechanism of IspH catalysis led to the rational design of potent inhibitors that target both IspH and IspG. The "rational" aspect is that, with IspH, we are proposing the formation of π-complexes with olefins and allyl anions, in which case it might be expected that other species—acetylenes—would also bind to the $[Fe_4S_4]$ cluster. There is in fact precedent for the formation of organometallic species between synthetic $[Fe_4S_4]$ clusters and alkynes. For example, McMillan et al. proposed the formation of an organometallic species containing a side-on acetylene unit to account for the *cis* reduction of acetylene to ethylene by the reduced cluster $[Fe_4S_4(SPh)_4]^{3-}$.[87] More direct evidence for the formation of π-complexes comes from the significant shifts of the vibrational Raman spectra of acetylene when bound to a reduced $[Fe_4S_4]$ cluster.[88] The binding and inhibition of IspH (and IspG) by propargyl alcohol (**19**) as well as the series of alkyne diphosphates **20**–**23** and their isoelectronic analogues **24** and **25** (Scheme 11) was thus investigated.[24,66,89] As expected, **19**

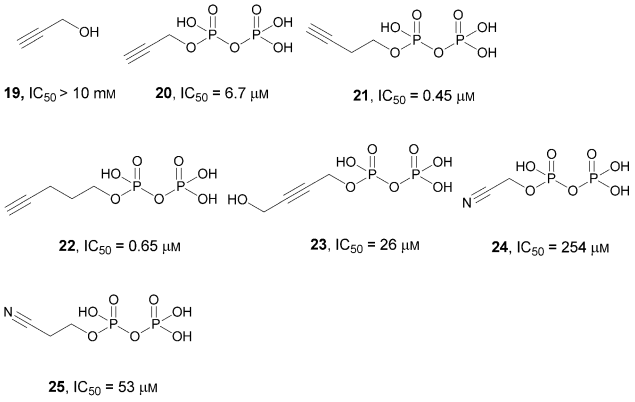

Scheme 11. Alkyne and cyano diphosphate inhibitors investigated.[89]

binds to reduced IspH, as evidenced by EPR spectroscopic data, which indicate large *g*-value changes (Figure 9a), although **19** has poor inhibitory activity against IspH. This activity improved upon the addition of a diphosphate group: the resulting propargyl diphosphate **20** has an IC_{50} value of 6.7 μM against *A. aeolicus* IspH.[24] Like **19**, **20** changed the

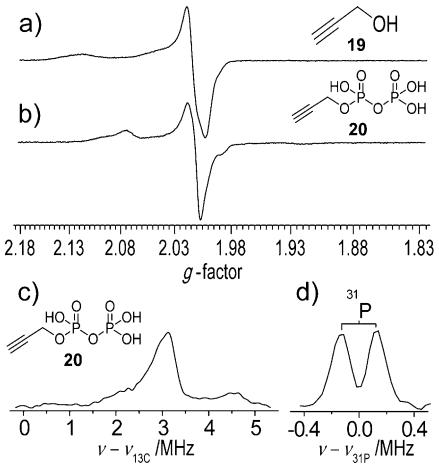

Figure 9. Binding of propargyl alcohol (**19**) and propargyl diphosphate (**20**) to reduced *A. aeolicus* IspH. a,b) X-band EPR spectra of **19** and **20** bound to *A. aeolicus* IspH. c,d) X-band ^{13}C and ^{31}P ENDOR spectra of **20** bound to *A. aeolicus* IspH. Adapted from Ref. [24] with permission.

EPR spectrum of IspH (Figure 9b), and an $A(^{13}C)$ value of about 6 MHz was observed by ENDOR spectroscopy when [U-$^{13}C_3$]**19** or [U-$^{13}C_3$]**20** were used (Figure 9c). Only a very small ^{31}P hyperfine coupling constant (ca. 0.3 MHz) was observed with **20**, thus indicating that the diphosphate group does not bind to the $[Fe_4S_4]^+$ cluster (Figure 9d). The best acetylenic inhibitor found to date is **21** with an IC_{50} value of 0.45 μM ($K_i \approx 60$ nM) against *A. aeolicus* IspH.[89] The isoelectronic cyano diphosphates **24** and **25** both showed much weaker inhibitory effects when compared with their alkyne diphosphate counterparts.

The alkyne diphosphates also turned out to be potent inhibitors of IspG. For example, **20** is a competitive IspG inhibitor with an IC_{50} value of 0.75 μM ($K_i \approx 330$ nM).[33,66] The EPR spectrum of **20** bound to IspG was similar to that observed for **20** bound to IspH, and the ENDOR spectrum exhibited a significant ($A(^{13}C) \approx 7$ MHz) hyperfine interaction when [U-$^{13}C_3$]**20** was added to reduced IspG, a result consistent with the formation of a π-complex.[66]

5.3. Screening of Compound Libraries

A third class of IspH inhibitors, pyridine diphosphates (compounds **26** and **27**; Scheme 12), were discovered by screening a library of diphosphates and bisphosphonates

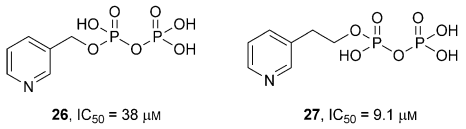

26, IC_{50} = 38 μM **27**, IC_{50} = 9.1 μM

Scheme 12. Pyridine diphosphate inhibitors of *A. aeolicus* IspH.[89]

previously developed as prenyl synthase inhibitors.[89] These compounds bind directly to the $[Fe_4S_4]^+$ cluster of *A. aeolicus* IspH through the nitrogen atom of the pyridine moiety, as evidenced by the change in the EPR spectrum on ligand addition (Figure 10a), and more importantly, by the presence of a large ^{14}N hyperfine coupling observed in HYSCORE spectra of *A. aeolicus* IspH bound to **26** (Figure 10b) or **27**.[90] The ^{14}N hyperfine-coupling tensor of the pyridine nitrogen atom of $A = [6.2, 7.6, 8.4]$ MHz and the nuclear quadrupole coupling constant of $e^2qQ/h = 3.0$ MHz are both comparable to the values found in other systems containing known Fe–N bonds.[90] However, these pyridine diphosphates were only weak inhibitors of *E. coli* IspH ($IC_{50} = 0.5$ mM for **26**).

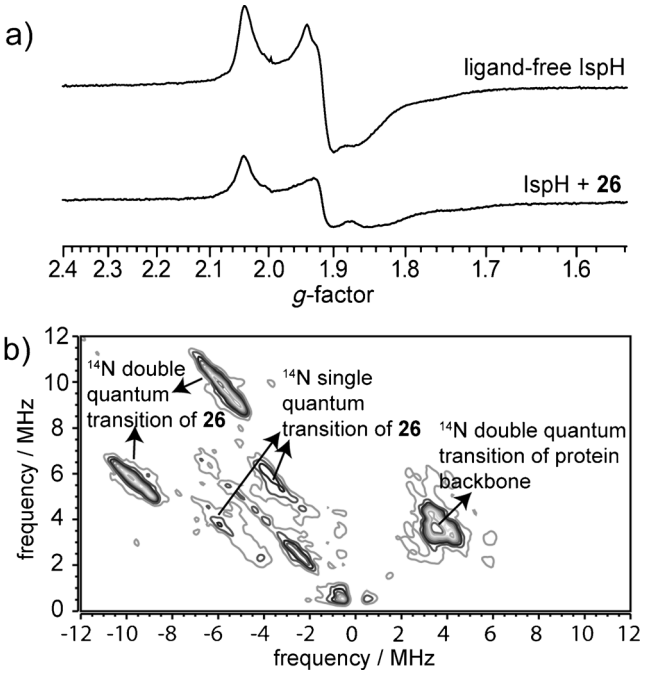

Figure 10. X-band EPR and HYSCORE spectra of reduced IspH with the pyridine inhibitor **26**. a) EPR spectra of ligand-free *A. aeolicus* IspH (top) and *A. aeolicus* IspH + **26** (bottom). b) HYSCORE spectrum of reconstituted *A. aeolicus* IspH + **26**. Adapted from Ref. [90] with permission. Copyright (2011) American Chemical Society.

6. Acetylene Hydratase Activity of IspH

To learn more about how these acetylenic inhibitors might bind to IspH, X-ray crystallographic structure analysis of **20**–**22** bound to oxidized IspH was carried out as a prelude to structural determination of their binding to reduced IspH. The results revealed that the binding of **20**–**22** to oxidized IspH was quite different to the binding mode proposed for the reduced enzyme. More significantly, unexpected hydratase activity of IspH was discovered, whereby oxidized IspH converts **21** into an aldehyde and **22** into a ketone (Scheme 13).[91]

The crystal structure of **20** bound to oxidized IspH (Figure 11a; PDB: 3URK) shows that the acetylenic carbon atoms of **20** are 3.4 and 3.6 Å away from the unique fourth iron center. Furthermore, there is a water molecule (or a hydroxide ion) bound to the $[Fe_4S_4]$ cluster with a Fe–O bond length of 2.1 Å: essentially the same Fe–O distance as is found when **4** is bound to oxidized IspH.[35,36]

The X-ray crystal structures of IspH in complex with **21** or **22** were even more surprising, since they showed that both ligands had undergone a hydration reaction. The crystal structure of IspH co-crystallized with **21** indicated the formation of the η^1-enolate complex **28** by anti-Markovnikov addition, and again there was a 2.0 Å Fe–O bond length (Figure 11b; PDB: 3UTC). This complex was found to actually turn over, and the aldehyde **29** was detected.[91] In the case of **22**, the crystal structure again revealed a chemical reaction of the acetylene group (Figure 11c; PDB: 3UTD), but rather than the formation of an aldehyde, the X-ray crystallographic results now indicated Markovnikov addition, with formation of the ketone **30**.[91]

The reactions catalyzed by IspH are summarized in Scheme 13. All substrates contain a diphosphate group, which binds to the conserved diphosphate binding site[19,47] and position C4 of ligands close to the unique fourth Fe center of the oxidized cluster ($[Fe_4S_4]^{2+}$). Thus, with **20**, the C_3 side chain is too short to interact with the unique fourth Fe atom

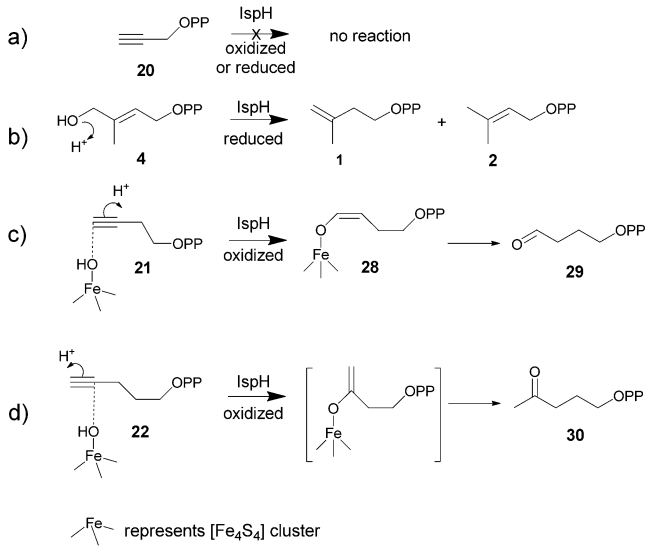

Scheme 13. Summary of IspH reactions.

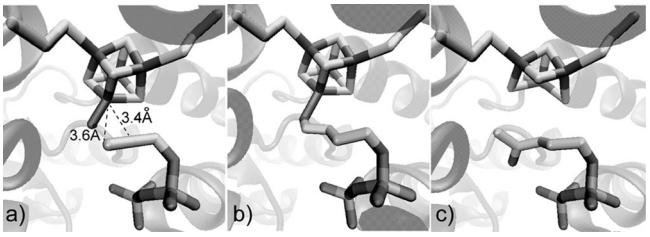

Figure 11. X-ray crystal structures of alkynyl diphosphates or their products (derived by transformation by the enzyme) bound to *E. coli* IspH. a) Compound **20** bound to *E. coli* IspH. b) Enolate **28** (derived from **21**) with *E. coli* IspH. c) Ketone **30** (derived from **22**) with *E. coli* IspH. The images were prepared with VMD.[38]

(Scheme 13a); however, with the C_4 species **21**, OH (presumably from a cluster-bound water molecule, as seen in the structure of IspH:**20**) adds to C4 through anti-Markovnikov addition to form the η^1-enolate **28**, which is then released as the aldehyde **29** (Scheme 13c). With a C_5 side chain (compound **22**), OH once again adds at C4, but now, protonation must be at C5 (Markovnikov addition), thus resulting in the formation of ketone **30** (Scheme 13d).

The hydration/dehydration reaction is one of the well-known functions catalyzed by the $[Fe_4S_4]$ clusters in several proteins (such as aconitase),[5] and in the case of *E. coli* fumarase A (FumA), the enzyme is also capable of catalyzing the hydration of an acetylene, acetylene dicarboxylate,[5,92,93] to oxaloacetate. In the tungsten–$[Fe_4S_4]$-containing acetylene hydratase from *Pelobacter acetylenicus*, the $[Fe_4S_4]$ cluster plays an indirect role in catalysis by increasing the pK_a value of an Asp residue at the active site.[94,95] The electron-transfer function of $[Fe_4S_4]$ may also facilitate the dehydration reaction, as demonstrated for 2-hydroxyglutaryl-CoA dehydratase from *Clostridium symbiosum*, which dehydrates its substrate via a ketyl radical intermediate.[96] In light of these examples, the hydratase activity of IspH is not a surprise: although optimized by nature to function as a $2H^+/2e^-$ deoxygenase, when an appropriate ligand is positioned in the right location, IspH can also exhibit hydratase activity—one of the intrinsic activities of $[Fe_4S_4]$ clusters.

7. Summary and Outlook

The structures and mechanisms of action of the $[Fe_4S_4]$-cluster-containing enzymes IspG and IspH have been of considerable interest for many years because these enzymes produce the C_5 "building blocks" IPP (**1**) and DMAPP (**2**) of the largest class of small organic molecules on Earth: the terpenes. Understanding of their structures, mechanisms of action, and inhibition could lead to new drugs as well as new herbicides. IspG and IspH both catalyze $2H^+/2e^-$ reductions, most likely via bioorganometallic reaction intermediates. In IspG catalysis, we propose that a ferraoxetane intermediate containing Fe–C and Fe–O bonds is involved; in IspH catalysis, a weak π-complex and an allyl η^3-complex are involved. The mechanisms proposed are the first examples of bioorganometallic catalytic mechanisms of $[Fe_4S_4]$ enzymes. They led to the design of the first potent IspH and IspG inhibitors: alkyne diphosphates. Additional inhibitors have been discovered by compound-library screening and the synthesis of substrate analogues. These novel inhibitors open up potentially new routes to the design of anti-infective drugs that target $[Fe_4S_4]$-containing proteins in the MEP pathway for isoprenoid biosynthesis.

There are, however, still many unanswered questions. From a structural perspective, key questions include: What are the exact structures of the three-domain IspGs? Which ligands are bound to the cluster in oxidized IspH in the absence of an exogenous ligand? Can one obtain crystal structures of the reaction intermediates? From a functional perspective, several important aspects still need to be addressed. First, although high activity has been achieved by using dithionite and artificial electron mediators,[18] the native redox system remains elusive. How relevant, then, are these model redox systems to the situation found in cells? Second, there is a need for more detailed studies of the pre-steady-state kinetics of the proposed reaction intermediates. Third, the proposed HiPIP-like intermediates need to be trapped in high yield for further characterization (e.g. by Mössbauer spectroscopy) to test their HiPIP-like nature. From the perspective of inhibitor design: Can one obtain potent IspG/IspH inhibitors that are active in cells and in vivo? Would an IspH-specific inhibitor be a good or a bad thing? It could certainly kill the targeted pathogens, and the concomitant accumulation of **4** would activate $\gamma\delta$ T cells (containing the Vγ2Vδ2 T-cell receptor), but this activity could be too much of a good thing, since it could lead to sepsis.[97] Therefore, IspG or combined IspH + IspG inhibitors might be required, for safety and efficacy.

The results on oxidized IspH also suggest an exciting link between the $[Fe_4S_4]$ clusters in IspH and other $[Fe_4S_4]$ proteins that are drug/herbicide targets. For example, the fact that IspH and FumA hydrate acetylenes in the same way is of interest, since FumA in malaria parasites is a drug target.[98]

Likewise, the enzymes dihydroxyacid dehydratase (DHAD)[99] and isopropylmalate isomerase (IPMI)[100] are targets for the inhibition of the biosynthesis of branched-chain amino acids in tuberculosis bacteria (inside macrophages) and are also of interest as herbicide targets; diverse inhibitors have been reported.[101] Some of these compounds may also inhibit IspH and IspG, whereas the leads that inhibit IspH and IspG may provide new ideas for DHAD and IPMI inhibitors, all with $[Fe_4S_4]$ clusters containing a unique fourth iron atom as their targets.

Acknowledgement

This research was supported by the United States Public Health Service (NIH grant GM065307). W.W. was supported by an American Heart Association, Midwest Affiliate, Predoctoral Fellowship (10PRE4430022). We are grateful to our collaborators and colleagues for many lively discussions, and to Jeroen S. Dickschat and the reviewers for their critical reading of the manuscript and their valuable suggestions.

Received: August 1, 2013
Published online: January 31, 2014

[1] H. Beinert, R. H. Holm, E. Munck, *Science* **1997**, *277*, 653 – 659.
[2] M. Bruschi, F. Guerlesquin, *FEMS Microbiol. Lett.* **1988**, *54*, 155 – 175.
[3] S. Ciurli, F. Musiani, *Photosynth. Res.* **2005**, *85*, 115 – 131.
[4] H. Beinert, M. C. Kennedy, C. D. Stout, *Chem. Rev.* **1996**, *96*, 2335 – 2374.
[5] D. H. Flint, R. M. Allen, *Chem. Rev.* **1996**, *96*, 2315 – 2334.
[6] H. J. Sofia, G. Chen, B. G. Hetzler, J. F. Reyes-Spindola, N. E. Miller, *Nucleic Acids Res.* **2001**, *29*, 1097 – 1106.
[7] M. Rohmer, *Lipids* **2008**, *43*, 1095 – 1107.
[8] M. Rohmer, *Nat. Prod. Rep.* **1999**, *16*, 565 – 574.
[9] W. Eisenreich, A. Bacher, D. Arigoni, F. Rohdich, *Cell. Mol. Life Sci.* **2004**, *61*, 1401 – 1426.
[10] M. Rohmer, C. Grosdemange-Billiard, M. Seemann, D. Tritsch, *Curr. Opin. Invest. Drugs* **2004**, *5*, 154 – 162.
[11] H. K. Lichtenthaler, *Annu. Rev. Plant Physiol. Plant Mol. Biol.* **1999**, *50*, 47 – 65.
[12] P. Adam, S. Hecht, W. Eisenreich, J. Kaiser, T. Grawert, D. Arigoni, A. Bacher, F. Rohdich, *Proc. Natl. Acad. Sci. USA* **2002**, *99*, 12108 – 12113.
[13] B. Altincicek, E. C. Duin, A. Reichenberg, R. Hedderich, A. K. Kollas, M. Hintz, S. Wagner, J. Wiesner, E. Beck, H. Jomaa, *FEBS Lett.* **2002**, *532*, 437 – 440.
[14] M. Wolff, M. Seemann, B. T. S. Bui, Y. Frapart, D. Tritsch, A. G. Estrabot, M. Rodríguez-Concepción, A. Boronat, A. Marquet, M. Rohmer, *FEBS Lett.* **2003**, *541*, 115 – 120.
[15] F. Rohdich, F. Zepeck, P. Adam, S. Hecht, J. Kaiser, R. Laupitz, T. Grawert, S. Amslinger, W. Eisenreich, A. Bacher, D. Arigoni, *Proc. Natl. Acad. Sci. USA* **2003**, *100*, 1586 – 1591.
[16] T. Gräwert, J. Kaiser, F. Zepeck, R. Laupitz, S. Hecht, S. Amslinger, N. Schramek, E. Schleicher, S. Weber, M. Haslbeck, J. Buchner, C. Rieder, D. Arigoni, A. Bacher, W. Eisenreich, F. Rohdich, *J. Am. Chem. Soc.* **2004**, *126*, 12847 – 12855.
[17] R. C. Röhrich, N. Englert, K. Troschke, A. Reichenberg, M. Hintz, F. Seeber, E. Balconi, A. Aliverti, G. Zanetti, U. Köhler, M. Pfeiffer, E. Beck, H. Jomaa, J. Wiesner, *FEBS Lett.* **2005**, *579*, 6433 – 6438.
[18] Y. Xiao, L. Chu, Y. Sanakis, P. Liu, *J. Am. Chem. Soc.* **2009**, *131*, 9931 – 9933.
[19] T. Gräwert, F. Rohdich, I. Span, A. Bacher, W. Eisenreich, J. Eppinger, M. Groll, *Angew. Chem.* **2009**, *121*, 5867 – 5870; *Angew. Chem. Int. Ed.* **2009**, *48*, 5756 – 5759.
[20] K. Janthawornpong, S. Krasutsky, P. Chaignon, M. Rohmer, C. D. Poulter, M. Seemann, *J. Am. Chem. Soc.* **2013**, *135*, 1816 – 1822.
[21] W. Xu, N. S. Lees, D. Hall, D. Welideniya, B. M. Hoffman, E. C. Duin, *Biochemistry* **2012**, *51*, 4835 – 4849.
[22] C. Cole, J. D. Barber, G. J. Barton, *Nucleic Acids Res.* **2008**, *36*, W197 – 201.
[23] W. S. J. Valdar, *Proteins Struct. Funct. Bioinf.* **2002**, *48*, 227 – 241.
[24] W. Wang, K. Wang, Y.-L. Liu, J. H. No, M. J. Nilges, E. Oldfield, *Proc. Natl. Acad. Sci. USA* **2010**, *107*, 4522 – 4527.
[25] S. Hecht, W. Eisenreich, P. Adam, S. Amslinger, K. Kis, A. Bacher, D. Arigoni, F. Rohdich, *Proc. Natl. Acad. Sci. USA* **2001**, *98*, 14837 – 14842.
[26] M. Seemann, B. T. Bui, M. Wolff, D. Tritsch, N. Campos, A. Boronat, A. Marquet, M. Rohmer, *Angew. Chem.* **2002**, *114*, 4513 – 4515; *Angew. Chem. Int. Ed.* **2002**, *41*, 4337 – 4339.
[27] F. Zepeck, T. Grawert, J. Kaiser, N. Schramek, W. Eisenreich, A. Bacher, F. Rohdich, *J. Org. Chem.* **2005**, *70*, 9168 – 9174.
[28] M. Seemann, B. T. S. Bui, M. Wolff, M. Miginiac-Maslow, M. Rohmer, *FEBS Lett.* **2006**, *580*, 1547 – 1552.
[29] Y. Xiao, G. Zahariou, Y. Sanakis, P. Liu, *Biochemistry* **2009**, *48*, 10483 – 10485.
[30] M. Lee, T. Gräwert, F. Quitterer, F. Rohdich, J. Eppinger, W. Eisenreich, A. Bacher, M. Groll, *J. Mol. Biol.* **2010**, *404*, 600 – 610.
[31] W. Xu, N. S. Lees, D. Adedeji, J. Wiesner, H. Jomaa, B. M. Hoffman, E. C. Duin, *J. Am. Chem. Soc.* **2010**, *132*, 14509 – 14520.
[32] A. K. Kollas, E. C. Duin, M. Eberl, B. Altincicek, M. Hintz, A. Reichenberg, D. Henschker, A. Henne, I. Steinbrecher, D. N. Ostrovsky, R. Hedderich, E. Beck, H. Jomaa, J. Wiesner, *FEBS Lett.* **2002**, *532*, 432 – 436.
[33] Y.-L. Liu, F. Guerra, K. Wang, W. Wang, J. Li, C. Huang, W. Zhu, K. Houlihan, Z. Li, Y. Zhang, S. K. Nair, E. Oldfield, *Proc. Natl. Acad. Sci. USA* **2012**, *109*, 8558 – 8563.
[34] K. Okada, T. Hase, *J. Biol. Chem.* **2005**, *280*, 20672 – 20679.
[35] I. Rekittke, J. Wiesner, R. Röhrich, U. Demmer, E. Warkentin, W. Xu, K. Troschke, M. Hintz, J. H. No, E. C. Duin, E. Oldfield, H. Jomaa, U. Ermler, *J. Am. Chem. Soc.* **2008**, *130*, 17206 – 17207.
[36] T. Gräwert, I. Span, W. Eisenreich, F. Rohdich, J. Eppinger, A. Bacher, M. Groll, *Proc. Natl. Acad. Sci. USA* **2010**, *107*, 1077 – 1081.
[37] M. Seemann, K. Janthawornpong, J. Schweizer, L. H. Bottger, A. Janoschka, A. Ahrens-Botzong, E. N. Tambou, O. Rotthaus, A. X. Trautwein, M. Rohmer, V. Schunemann, *J. Am. Chem. Soc.* **2009**, *131*, 13184 – 13185.
[38] W. Humphrey, A. Dalke, K. Schulten, *J. Mol. Graphics* **1996**, *14*, 33 – 38.
[39] I. Rekittke, T. Nonaka, J. Wiesner, U. Demmer, E. Warkentin, H. Jomaa, U. Ermler, *FEBS Lett.* **2011**, *585*, 447 – 451.
[40] R. R. Copley, P. Bork, *J. Mol. Biol.* **2000**, *303*, 627 – 641.
[41] K. E. Hevener, M. K. Yun, J. Qi, I. D. Kerr, K. Babaoglu, J. G. Hurdle, K. Balakrishna, S. W. White, R. E. Lee, *J. Med. Chem.* **2010**, *53*, 166 – 177.
[42] T. F. Oliveira, C. Vonrhein, P. M. Matias, S. S. Venceslau, I. A. Pereira, M. Archer, *J. Biol. Chem.* **2008**, *283*, 34141 – 34149.
[43] U. Swamy, M. Wang, J. N. Tripathy, S. K. Kim, M. Hirasawa, D. B. Knaff, J. P. Allen, *Biochemistry* **2005**, *44*, 16054 – 16063.
[44] I. Rekittke, H. Jomaa, U. Ermler, *FEBS Lett.* **2012**, *586*, 3452 – 3457.

[45] M. Seemann, P. Wegner, V. Schunemann, B. T. Bui, M. Wolff, A. Marquet, A. X. Trautwein, M. Rohmer, *J. Biol. Inorg. Chem.* **2005**, *10*, 131 – 137.
[46] Y. Xiao, Z. K. Zhao, P. Liu, *J. Am. Chem. Soc.* **2008**, *130*, 2164 – 2165.
[47] T. Gräwert, I. Span, A. Bacher, M. Groll, *Angew. Chem.* **2010**, *122*, 8984 – 8991; *Angew. Chem. Int. Ed.* **2010**, *49*, 8802 – 8809.
[48] W. C. Chang, Y. Xiao, H. W. Liu, P. Liu, *Angew. Chem.* **2011**, *123*, 12512 – 12515; *Angew. Chem. Int. Ed.* **2011**, *50*, 12304 – 12307.
[49] Y. Xiao, W. C. Chang, H. W. Liu, P. Liu, *Org Lett.* **2011**, *13*, 5912 – 5915.
[50] W. Wang, K. Wang, I. Span, J. Jauch, A. Bacher, M. Groll, E. Oldfield, *J. Am. Chem. Soc.* **2012**, *134*, 11225 – 11234.
[51] A. Ahrens-Botzong, K. Janthawornpong, J. A. Wolny, E. N. Tambou, M. Rohmer, S. Krasutsky, C. D. Poulter, V. Schunemann, M. Seemann, *Angew. Chem.* **2011**, *123*, 12182 – 12185; *Angew. Chem. Int. Ed.* **2011**, *50*, 11976 – 11979.
[52] I. Span, T. Gräwert, A. Bacher, W. Eisenreich, M. Groll, *J. Mol. Biol.* **2012**, *416*, 1 – 9.
[53] M. M. Werst, M. C. Kennedy, H. Beinert, B. M. Hoffman, *Biochemistry* **1990**, *29*, 10526 – 10532.
[54] M. C. Kennedy, M. Werst, J. Telser, M. H. Emptage, H. Beinert, B. M. Hoffman, *Proc. Natl. Acad. Sci. USA* **1987**, *84*, 8854 – 8858.
[55] C. A. Citron, N. L. Brock, P. Rabe, J. S. Dickschat, *Angew. Chem.* **2012**, *124*, 4129 – 4133; *Angew. Chem. Int. Ed.* **2012**, *51*, 4053 – 4057.
[56] H. I. Lee, R. Y. Igarashi, M. Laryukhin, P. E. Doan, P. C. Dos Santos, D. R. Dean, L. C. Seefeldt, B. M. Hoffman, *J. Am. Chem. Soc.* **2004**, *126*, 9563 – 9569.
[57] V. Pelmenschikov, D. A. Case, L. Noodleman, *Inorg. Chem.* **2008**, *47*, 6162 – 6172.
[58] J. A. J. Jarvis, B. T. Kilbourn, P. G. Owston, *Acta Crystallogr. Sect. B* **1971**, *27*, 366 – 372.
[59] J. Li, K. Wang, T. I. Smirnova, R. L. Khade, Y. Zhang, E. Oldfield, *Angew. Chem.* **2013**, *125*, 6650 – 6653; *Angew. Chem. Int. Ed.* **2013**, *52*, 6522 – 6525.
[60] L. Zhao, W. C. Chang, Y. Xiao, H. W. Liu, P. Liu, *Annu. Rev. Biochem.* **2013**, *82*, 497 – 530.
[61] H. J. McManus, R. W. Fessenden, D. M. Chipman, *J. Phys. Chem.* **1988**, *92*, 3778 – 3781.
[62] M. Belinskii, *Chem. Phys.* **1993**, *172*, 189 – 211.
[63] C. R. Staples, E. Ameyibor, W. Fu, L. Gardet-Salvi, A. L. Stritt-Etter, P. Schurmann, D. B. Knaff, M. K. Johnson, *Biochemistry* **1996**, *35*, 11425 – 11434.
[64] C. R. Staples, E. Gaymard, A. L. Stritt-Etter, J. Telser, B. M. Hoffman, P. Schurmann, D. B. Knaff, M. K. Johnson, *Biochemistry* **1998**, *37*, 4612 – 4620.
[65] E. M. Walters, R. Garcia-Serres, G. N. Jameson, D. A. Glauser, F. Bourquin, W. Manieri, P. Schurmann, M. K. Johnson, B. H. Huynh, *J. Am. Chem. Soc.* **2005**, *127*, 9612 – 9624.
[66] W. Wang, J. Li, K. Wang, C. Huang, Y. Zhang, E. Oldfield, *Proc. Natl. Acad. Sci. USA* **2010**, *107*, 11189 – 11193.
[67] W. Wang, K. Wang, J. Li, S. Nellutla, T. I. Smirnova, E. Oldfield, *J. Am. Chem. Soc.* **2011**, *133*, 8400 – 8403.
[68] I. Span, K. Wang, W. Wang, J. Jauch, W. Eisenreich, A. Bacher, E. Oldfield, M. Groll, *Angew. Chem.* **2013**, *125*, 2172 – 2175; *Angew. Chem. Int. Ed.* **2013**, *52*, 2118 – 2121.
[69] W. Brandt, M. A. Dessoy, M. Fulhorst, W. Gao, M. H. Zenk, L. A. Wessjohann, *ChemBioChem* **2004**, *5*, 311 – 323.
[70] Y. Xiao, D. Rooker, Q. You, C. L. Meyers, P. Liu, *ChemBioChem* **2011**, *12*, 527 – 530.
[71] T. Itoh, T. Nagano, M. Sato, M. Hirobe, *Tetrahedron Lett.* **1989**, *30*, 6387 – 6388.
[72] R. L. Nyland II, Y. Xiao, P. Liu, C. L. F. Meyers, *J. Am. Chem. Soc.* **2009**, *131*, 17734 – 17735.
[73] Y. Xiao, R. L. Nyland II, C. L. F. Meyers, P. Liu, *Chem. Commun.* **2010**, *46*, 7220 – 7222.
[74] D. Adedeji, H. Hernandez, J. Wiesner, U. Kohler, H. Jomaa, E. C. Duin, *FEBS Lett.* **2007**, *581*, 279 – 283.
[75] A. Silakov, B. Wenk, E. Reijerse, S. P. Albracht, W. Lubitz, *J. Biol. Inorg. Chem.* **2009**, *14*, 301 – 313.
[76] A. S. Hashmi, G. J. Hutchings, *Angew. Chem.* **2006**, *118*, 8064 – 8105; *Angew. Chem. Int. Ed.* **2006**, *45*, 7896 – 7936.
[77] M. J. Calhorda, A. M. Galvao, C. Unaleroglu, A. A. Zlota, F. Frolow, D. Milstein, *Organometallics* **1993**, *12*, 3316 – 3325.
[78] Z. H. Kafafi, R. H. Hauge, W. E. Billups, J. L. Margrave, *J. Am. Chem. Soc.* **1987**, *109*, 4775 – 4780.
[79] I. Bertini, F. Capozzi, C. Luchinat, M. Piccioli, A. J. Vila, *J. Am. Chem. Soc.* **1994**, *116*, 651 – 660.
[80] L. Charon, J. F. Hoeffler, C. Pale-Grosdemange, L. M. Lois, N. Campos, A. Boronat, M. Rohmer, *Biochem. J.* **2000**, *346*, 737 – 742.
[81] E. Oldfield, *Acc. Chem. Res.* **2010**, *43*, 1216 – 1226.
[82] C. Obiol-Pardo, J. Rubio-Martinez, S. Imperial, *Curr. Med. Chem.* **2011**, *18*, 1325 – 1338.
[83] W. N. Hunter, *Curr. Top. Med. Chem.* **2011**, *11*, 2048 – 2059.
[84] S. Van Hoof, C. J. Lacey, R. C. Röhrich, J. Wiesner, H. Jomaa, S. Van Calenbergh, *J. Org. Chem.* **2008**, *73*, 1365 – 1370.
[85] A. Reichenberg, M. Hintz, Y. Kletschek, T. Kuhl, C. Haug, R. Engel, J. Moll, D. N. Ostrovsky, H. Jomaa, M. Eberl, *Bioorg. Med. Chem. Lett.* **2003**, *13*, 1257 – 1260.
[86] M. Eberl, M. Hintz, A. Reichenberg, A.-K. Kollas, J. Wiesner, H. Jomaa, *FEBS Lett.* **2003**, *544*, 4 – 10.
[87] R. S. McMillan, J. Renaud, J. G. Reynolds, R. H. Holm, *J. Inorg. Biochem.* **1979**, *11*, 213 – 227.
[88] K. Tanaka, M. Nakamoto, M. Tsunomori, T. Tanaka, *Chem. Lett.* **1987**, 613 – 616.
[89] K. Wang, W. Wang, J. H. No, Y. Zhang, Y. Zhang, E. Oldfield, *J. Am. Chem. Soc.* **2010**, *132*, 6719 – 6727.
[90] W. Wang, J. Li, K. Wang, T. I. Smirnova, E. Oldfield, *J. Am. Chem. Soc.* **2011**, *133*, 6525 – 6528.
[91] I. Span, K. Wang, W. Wang, Y. Zhang, A. Bacher, W. Eisenreich, K. Li, C. Schulz, E. Oldfield, M. Groll, *Nat. Commun.* **2012**, *3*, 1042.
[92] D. H. Flint, R. G. McKay, *J. Am. Chem. Soc.* **1994**, *116*, 5534.
[93] D. H. Flint, *Arch. Biochem. Biophys.* **1994**, *311*, 509 – 516.
[94] G. B. Seiffert, G. M. Ullmann, A. Messerschmidt, B. Schink, P. M. Kroneck, O. Einsle, *Proc. Natl. Acad. Sci. USA* **2007**, *104*, 3073 – 3077.
[95] F. Tenbrink, B. Schink, P. M. Kroneck, *J. Bacteriol.* **2011**, *193*, 1229 – 1236.
[96] A. Parthasarathy, A. J. Pierik, J. Kahnt, O. Zelder, W. Buckel, *Biochemistry* **2011**, *50*, 3540 – 3550.
[97] M. S. Davey, C. Y. Lin, G. W. Roberts, S. Heuston, A. C. Brown, J. A. Chess, M. A. Toleman, C. G. Gahan, C. Hill, T. Parish, J. D. Williams, S. J. Davies, D. W. Johnson, N. Topley, B. Moser, M. Eberl, *PLoS Pathog.* **2011**, *7*, e1002040.
[98] V. Bulusu, V. Jayaraman, H. Balaram, *J. Biol. Chem.* **2011**, *286*, 9236 – 9245.
[99] V. Singh, D. Chandra, B. S. Srivastava, R. Srivastava, *Microbiology* **2011**, *157*, 38 – 46.
[100] K. Jensen, U. D. Ranganathan, K. K. Van Rompay, D. R. Canfield, I. Khan, R. Ravindran, P. A. Luciw, W. R. Jacobs, Jr., G. Fennelly, M. H. Larsen, K. Abel, *Clin. Vaccine Immunol.* **2012**, *19*, 1170 – 1181.
[101] D. H. Flint, A. Nudelman, *Bioorg. Chem.* **1993**, *21*, 367 – 385.

